Validating the strength algorithm for sub-arctic ice with field measurements from Labrador

Johnston, M.; Timco, G.

Publisher's version / Version de l'éditeur:
https://doi.org/10.4224/12327506
Technical Report (National Research Council of Canada. Canadian Hydraulics Centre); no. CHC-TR-032, 2005-03

Validating the Strength Algorithm for Sub-Arctic Ice with Field Measurements from Labrador

M. Johnston and G. Timco

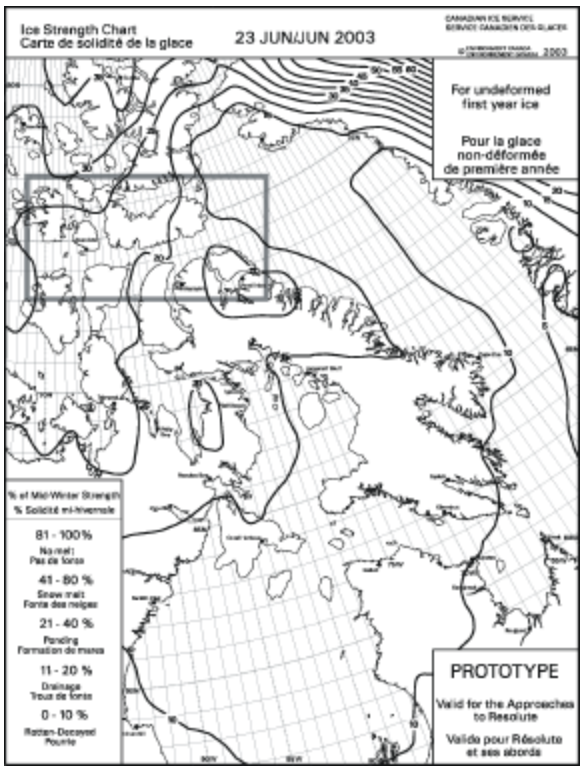

Technical Report, CHC-TR-032

March 2005

CHC CANADIAN HYDRAULICS CENTRE

Validating the Strength Algorithm for Sub-Arctic Ice with Field Measurements from Labrador

M. Johnston and G. Timco
Canadian Hydraulics Centre
National Research Council of Canada
Montreal Road
Ottawa, Ontario K1A 0R6

prepared for

Canadian Ice Service
373 Sussex Drive, Bld. E-3
Ottawa, Ontario K1A 0H3

Technical Report, CHC-TR-032

March 2005

Abstract

This report is the second of a two-year study that examines means by which to incorporate level, landfast first-year ice in the sub-Arctic into the Ice Strength Charts that are issued by the Canadian Ice Service during the summer months. It is suggested that, if sub-Arctic ice is to be included in future Ice Strength Charts, the contour lines of equal strength in the Charts should be based upon the calculated flexural strength of the ice. The most accurate approach for that calculation requires ice property measurements, which are not usually available. Alternately, a second approach was explored: data output from the thermodynamic model used by the Canadian Ice Service was used to calculate the flexural strength of the ice. Preliminary analysis showed that the air temperatures, snow and ice thickness, and ice temperatures forecast from the model were in reasonably good agreement with measurements made on first-year ice in the high Arctic and the sub-Arctic. It was suggested that output from the thermodynamic model could be used to calculate the flexural strength of first-year ice in the sub-Arctic until about mid-May, when the ice had about 35% of its maximum mid-winter strength. In the high Arctic, where the ice decay process is less complex, the forecasted data could be used to calculate the ice strength until early July, when the ice had about 10 to 15% of its maximum mid-winter strength.

Table of Contents

List of Figures

List of Tables

Validating the Strength Algorithm for Sub-Arctic Ice with Field Measurements from Labrador

1.0 Introduction

In the year 2000, the Canadian Hydraulics Centre (CHC) of the National Research Council Canada (NRC) began conducting measurements in the high Arctic, to provide much needed information about the properties of decaying sea ice during summer. To date, the authors have conducted three seasons of measurements on decaying first-year ice in the Arctic (Johnston et al., 2001; 2002; 2003). Those data provided the first systematic documentation of the changes that occur in sea ice during seasonal melt. That information had several important outcomes. The first outcome was the improved definition of "rotten" ice in terms of ice strength: first-year ice with melt holes throughout its full thickness, had only 10% of its mid-winter maximum strength (Timco and Johnston, 2002). The second outcome was the development of an Ice Strength Chart for level, landfast, first-year sea ice in the high Arctic. Each summer, the Canadian Ice Service (CIS) issues a series of Ice Strength Charts to forecast the seasonal decrease in the strength of first-year ice (Gauthier et al., 2002; Langlois et al., 2003). The Ice Strength Chart, an example of which is shown in Figure 1, is still in the prototype phase at CIS.

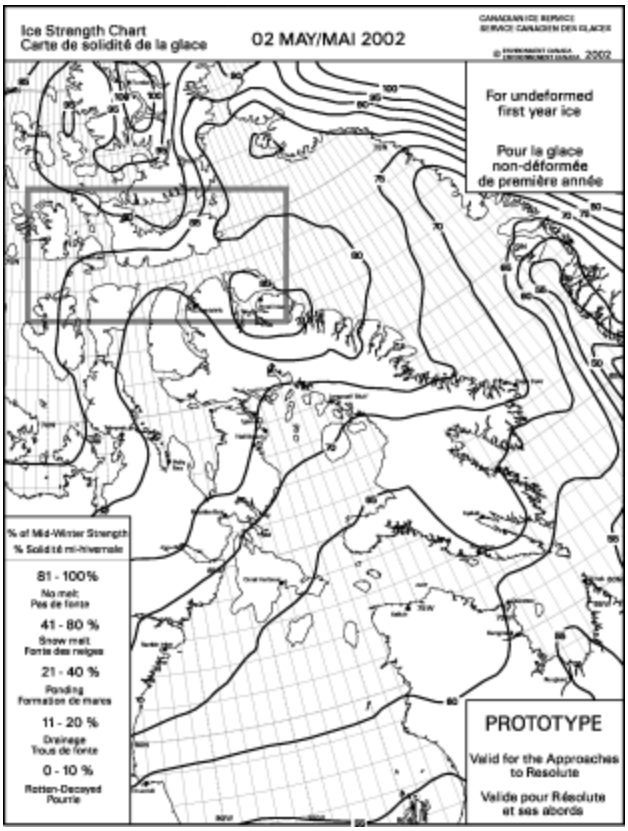

Figure 1 Prototype Ice Strength Chart issued by Canadian Ice Service

Field measurements showed that first-year ice at a number of sampling sites in the central Arctic (all at a latitude of about 74°N) underwent a similar seasonal decrease in strength. Since the Ice Strength Charts were based on sites that were sampled along the approach to Resolute, Nunavut (denoted by the grey box in Figure 1), the Charts state that the forecasted ice strength has the highest certainty in that region.

Currently, the Ice Strength Charts extend to the more temperate sub-Arctic ice, south of 60°N. There is little confidence in forecasting ice strength in that area, however. That is because only a limited number of property measurements have been conducted on sub-Arctic ice (Johnston and Timco, 2004). In the fall of 2003, the Canadian Hydraulics Centre (CHC) approached CIS about their interest in conducting measurements on first-year ice near Nain, Labrador, with the intention of using those measurements to develop a basis for incorporating sub-Arctic ice into the Ice Strength Charts. The response was positive. This report, the second of a two-year study, suggests an approach for including sub-Arctic level, landfast first-year ice into future Ice Strength Charts.

2.0 Ice Strength Charts: Past, Present and Future

In the year 2000, the CHC developed an approach to forecast the strength of level, landfast first-year ice in the high Arctic from air temperature data that were obtained from CIS using the Global Environmental Multi-scale (GEM) model[1]. Johnston and Timco (2003) present the analysis of three years of property measurements, which culminated in an Ice Strength Algorithm for first-year ice in the high Arctic. That algorithm, which formed the basis of the Ice Strength Charts, was an exponential equation that related ice strength to the accumulated degree-days (as determined from the mean daily air temperatures). The Ice Strength Algorithm was based on normalizing the measured ice borehole strength and the calculated flexural strength of the ice by their mid-winter maximum values. The normalized strengths were then plotted against the accumulated degree-days, and an exponential equation was fit through the curve.

While the Ice Strength Algorithm suggested by Johnston and Timco (2003) was appropriate for first-year ice in the high Arctic, it was not appropriate for sub-Arctic ice. Problems arose when it became necessary to select a normalizing factor that was appropriate for first-year ice at different latitudes (Johnston and Timco, 2004). Realizing that ice in sub-Arctic does not attain the thickness (or strength) of Arctic ice, the maximum mid-winter strength of Arctic first-year ice would not be appropriate for normalizing the strength of sub-Arctic ice. The second problem with the technique related to arriving at a single date from which to begin calculating the accumulated degree-days for the sub-Arctic and Arctic. Because air temperatures in the Arctic and sub-Arctic differ dramatically, there was no single date that completely captured the seasonal warming of the ice, yet minimized the effect that subzero air temperatures had on the accumulating degree-days. Analysis showed that when the technique for first-year ice in the high Arctic was applied to the sub-Arctic, the results erroneously implied that the strength of first-year ice in the sub-Arctic decreased *after* it did in the Arctic.

[1] Air temperatures output by the GEM model were shown to be in good agreement with air temperatures measured in the field (Johnston and Timco, 2003).

The authors concluded that, if Ice Strength Charts were to include first-year ice at different latitudes, the Charts should be based on calculating the flexural strength of the ice using either of the approaches presented in Timco and O'Brien (1994). The first, more accurate, approach (Approach A) uses depth-averages of the measured ice temperature and ice salinity for the calculation. The second approach (approach B) uses known information about the air temperature and the ice thickness to calculate the flexural strength. Since it is not possible, or practical, to measure the ice properties when needed, or to determine how they change with inter-annual variations in climate, it is suggested that the future Ice Strength Charts be based upon flexural strengths calculated using Approach B, or a similar approach.

One of the limitations of calculating the ice strength is that the equations can only be used up to a certain date. As the ice approaches near melting temperatures, its brine volume begins to increase exponentially, and neither Approach A nor Approach B can be used for the calculation. Herein lies the usefulness of measuring the *in situ* strength of the ice with the borehole indentor: the ice borehole strength can be measured when the flexural strength of the ice can no longer be calculated. Past work has shown that both the flexural and borehole strengths show a similar seasonal decrease, where the data overlap. Because the 2003 Ice Strength Algorithm was based (partly) on the relation between the measured borehole strength and the air temperature, it allowed CIS to produce Strength Charts for Arctic first-year ice after June (when the flexural strength could no longer be calculated using Approach B).

3.0 Outline of the Report

This report describes four different techniques for calculating the flexural strength of the ice (approaches A through D). Two of those approaches explore means by which to improve the accuracy of Approach B using actual ice thickness measurements, the measured *in situ* temperature of the ice, or output from the thermodynamic model used by CIS (Flato and Brown, 1996).

This report is structured as follows:

- Describe two main approaches for calculating the flexural strength of the ice. Demonstrate that using the measured ice properties for the calculation (Approach A) is preferred over using the air temperature and ice thickness (Approach B). Describe means of improving Approach B using measured, rather than approximated, ice temperatures.

- Illustrate similar trends in the seasonal decrease of the ice borehole strength and the calculated flexural strength of the ice. Discuss the usefulness of the borehole indentor for measuring the *in situ* strength of the ice, once the flexural strength can no longer be calculated.

- Examine recently acquired measurements from two regions of landfast, level first-year ice near Nain, Labrador. Use *in situ* temperature measurements to describe the response of first-year ice in the sub-Arctic and high Arctic to changes in the air temperature. Demonstrate that the relation between air temperature and bulk ice temperature is not a straightforward one.

- Validate output from the thermodynamic model used by CIS, with three seasons of field measurements from the Arctic and one season of data from the sub-Arctic.

- Compare the bulk ice temperatures obtained from *in situ* measurements in the Arctic and sub-Arctic to the bulk ice temperatures output from the thermodynamic model. The comparison will be used to determine the best approach for calculating the flexural strength of the ice.

- Discuss the limitations of using the calculated flexural strength to forecast ice strength late in the season. Those limitations can be addressed by developing a relation between the *in situ* borehole strength of the ice and the calculated flexural strength, which will require further analysis.

- Raise questions about the intended objectives of the Ice Strength Charts, and the way forward.

4.0 Approaches for Calculating the Flexural Strength of Ice

Several researchers have attempted to relate the strength of sea ice to the brine volume or total porosity of the ice. There is a good reason for this. It is generally assumed that as the total porosity in the ice increases, the strength should decrease. That is because there is less "solid ice" that has to be broken. Timco and O'Brien (1994) conducted the most comprehensive analysis of the flexural strength of ice. Their analysis was based upon approximately 1000 tests on sea ice, and used over 2500 reported measurements on the flexural strength of freshwater ice and sea ice. The authors showed that the data for first-year sea ice could be described by the following equation:

$$\sigma_f = 1.76 \exp\left(-5.88 * \sqrt{\upsilon_b}\right) \qquad (1)$$

where σ_f is the flexural strength of the ice and the brine volume (ν_b) is expressed as a brine volume fraction. This relationship is shown in Figure 2, using data that were compiled from a large number of investigators, and from a variety of geographic locations in both polar and temperate climates. Equation (1) should, therefore, be quite representative of the flexural strength of sea ice in most regions.

Equation (1) is the most comprehensive equation for flexural strength to date. There have been a few other equations proposed to relate strength and brine volume, however those were based on substantially fewer data points and data that extended over a very limited range. In other words, the other equations are valid over only a small brine volume range. The wider range of this equation represents these other equations very well in the regions where they are valid.

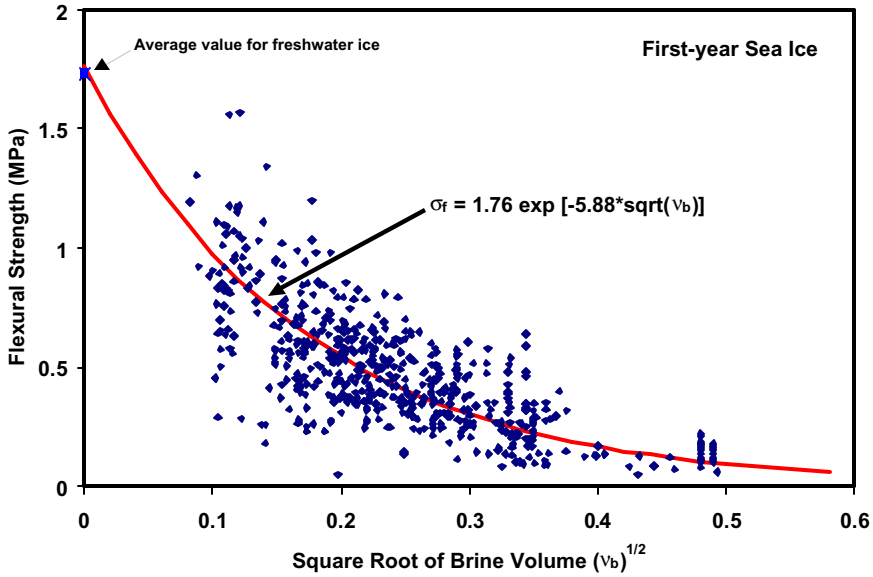

Figure 2 Flexural strength versus the square root of the brine volume for first-year sea ice (note that data do not exist to support the relation beyond a root brine volume of 0.5)

There are several points to note from Figure 2:

- The value of 1.76 MPa for zero brine volume is in excellent agreement with the average strength (1.73 MPa) measured for freshwater ice.
- The general scatter in the data increases with decreasing brine volume. This is a reflection of the fact that, at low brine volumes, the ice shows brittle behavior. The range of scatter approaches that measured for freshwater ice and is characteristic of a brittle material.
- Figure 2 shows there are no data to support using Equation (1) to calculate the flexural strength of sea ice when the root brine volume exceeds 0.5.
- The brine volume used to represent the ice beam for any test was taken as the average brine volume, determined from the average ice temperature and salinity of the beam.
- Calculating the flexural strength of an ice sheet would require the depth-averaged temperature of the ice (or bulk ice temperature) and depth-averaged salinity of the ice (bulk ice salinity).

4.1 Trends in Borehole Strength and Flexural Strength of Arctic Ice

Measuring the *in situ* borehole strength of the ice has been a fundamental part of the fieldwork on decaying sea ice. The borehole indentor offers distinct advantages over other types of strength measurements. First, borehole strength tests are performed in the 150 mm diameter hole left by the ice corer, which eliminates the need for sample preparation. Second, measurements have shown that borehole indentor tests are especially useful late in the season, when ice temperatures above –10°C make sample preparation extremely difficult. As such, the borehole strength has been an important part of understanding the physical process by which sea ice decays, and the reduction in ice strength.

Masterson (1996) gives a thorough description of the borehole jack and an interpretation of the strength that it provides. Since the ice borehole strength is a measure of the confined compressive strength of the ice, it is considerably higher than the flexural strength of the ice (which is an unconfined strength). For instance, the maximum (winter) ice borehole strength of Arctic first-year ice is about 29 MPa (Blanchet et al., 1997, Sinha 1986), whereas the maximum reported flexural strength of Arctic first-year ice is 0.71 MPa (Timco and O'Brien, 1994).

Figure 3 presents a summary of three seasons of measurements on level, landfast first-year ice in the high Arctic. The figure shows seasonal trends in the measured ice borehole strength, the calculated flexural strength of the ice, the snow and ice thickness, bulk ice temperature[2], bulk ice salinity[3], and the calculated brine volume fraction. Figure 3 shows that, as the ice decays, the ice borehole strength and the calculated flexural strength (using Approach A) decrease in a similar manner. As the bulk ice temperature increases, the bulk salinity of the extracted ice cores decreases, and the (calculated) brine volume fraction increases. The figure shows that the temperature, salinity and strength of decaying Arctic first-year ice change before the ice thickness begins to decrease. By 2 May (JD122), the ice had a borehole strength that was about 65% of its maximum winter strength. The ice borehole strength had decreased to 30% of its maximum strength by the time that above-freezing air temperatures were experienced, in mid-June (JD165), and to about 10 to 15% of its winter maximum by early July (JD183). The ice strength remained at the 10 to 15% level until the mid-August (JD223), when the last strength measurements were made on first-year ice.

[2] bulk ice temperature was obtained by depth averaging the *in situ* ice temperature data from Truro Island, 2002

[3] bulk ice salinity was depth averaged from measurements on extracted cores, as discussed in Appendix A.

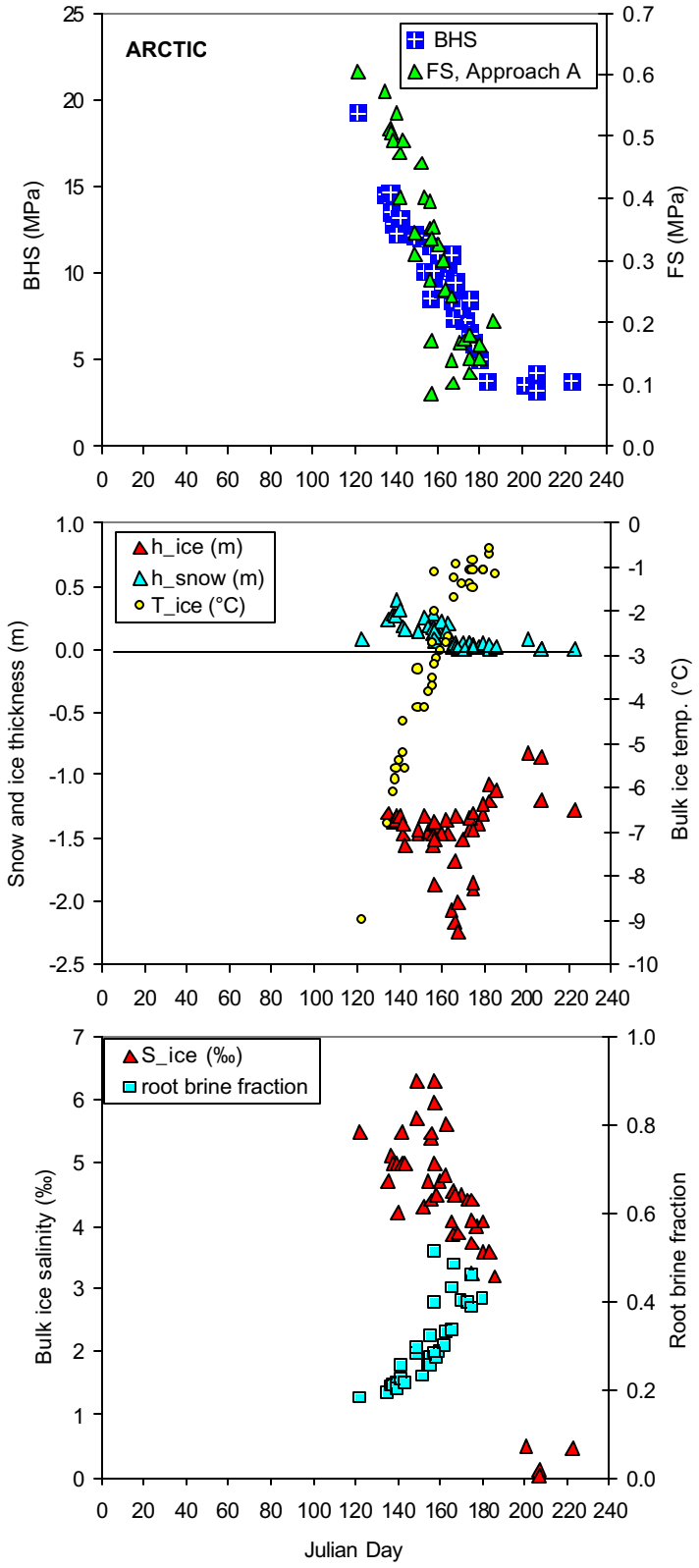

Figure 3 Seasonal trends in Arctic first-year ice

BHS: borehole strength FS: calculated flexural strength h_snow: snow thickness
T_ice: bulk ice temperature S_ice: bulk ice salinity h_ice: ice thickness

4.2 Calculating Flexural Strengths: Approach A vs. Approach B

The flexural strength reported in Figure 3 was calculated using Approach A (measured ice temperatures and ice salinity). When ice properties measurements are not available, Approach B must be used to calculate the flexural strength. That approach uses the air temperature to estimate the temperature of the top ice surface, which is then used to calculate the bulk temperature of the ice. The bulk ice salinity is calculated from information about the ice thickness.

Figure 4 shows the bulk temperature of first-year ice in the Arctic that was obtained from a temperature chain frozen into the ice versus the bulk ice temperature that was calculated using Approach B (from the air temperature and the ice thickness). All but two of the data points in the figure are below the line of 1:1 correspondence, which shows that Approach B underestimates the bulk temperature of the ice, compared to actual measurements. Data points that are directly on the x-axis indicate that Approach B cannot be used because the air temperatures was above 0°C. An underlying assumption of Approach B is that, when air temperatures are greater than -10°C, the air temperature equals the top ice surface temperature (which can not be greater than 0°C).

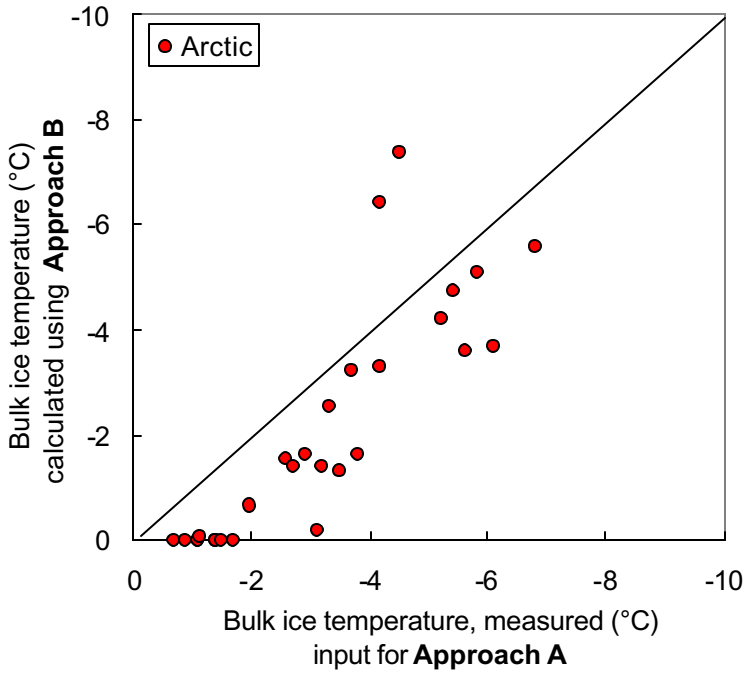

Figure 4 Bulk ice temperature: measured vs. using Approach B

Figure 5 shows the flexural strength calculated using Approach A and Approach B. There are several points to note from the figure. First, strengths calculated by Approach A and measured with the borehole indentor show a similar seasonal decrease. In comparison, strengths calculated using Approach B decrease more quickly than either of those two strengths. Also, for previously discussed reasons, Approach B is not valid when the air temperatures exceed 0°C. The figure shows that Approach B is not acceptable for calculating the strength of the ice at near melting temperatures (a state that aptly describes decaying ice). It should also be noted that in the figure, the strengths calculated using Approach B used the *measured* air temperature and the *measured* ice thickness -- therefore, they represent the highest accuracy with which the flexural strength can be calculated using that approach.

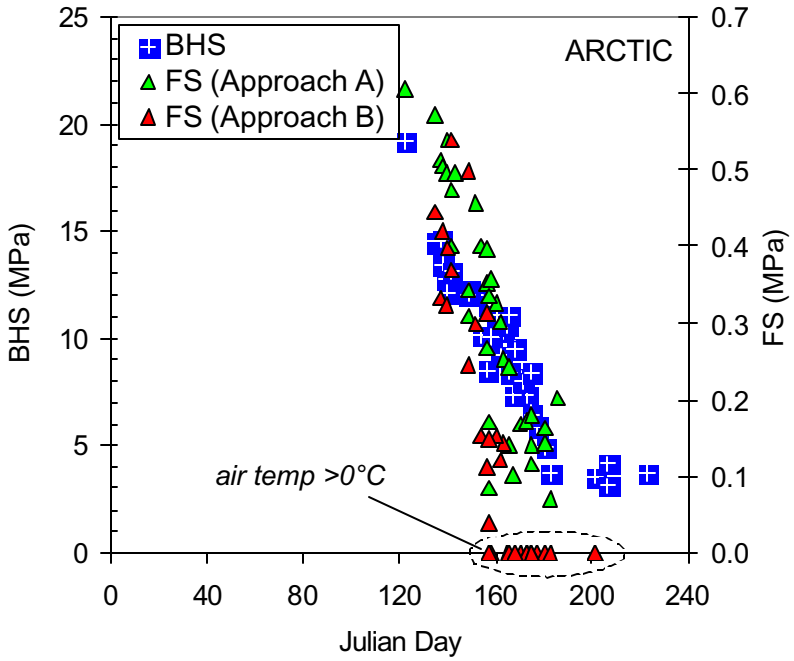

Figure 5 Ice borehole strength vs. flexural strength calculated using Approaches A and B

4.3 Approach C: A Modified Version of Approach B

Approach B leaves much to be desired when the flexural strength needs to be calculated late in the season, partly because it does not provide an accurate account of the bulk ice temperature or the brine volume. One means of improving Approach B would be to use the measured ice temperatures (when available) to override the bulk ice temperature calculated using Approach B. The modified approach will be called Approach C, and it will be explored using the bulk ice temperature obtained from *in situ* measurements, and the measured ice thickness.

Figure 6-a compares flexural strengths calculated using Approach A (measured bulk ice temperature and measured bulk ice salinity) to results from Approach C (using measured bulk ice temperature and measured ice thickness). As expected, flexural strengths calculated using Approach C agree more closely with those from Approach A, than the comparison between Approaches A and B (Figure 6-b).

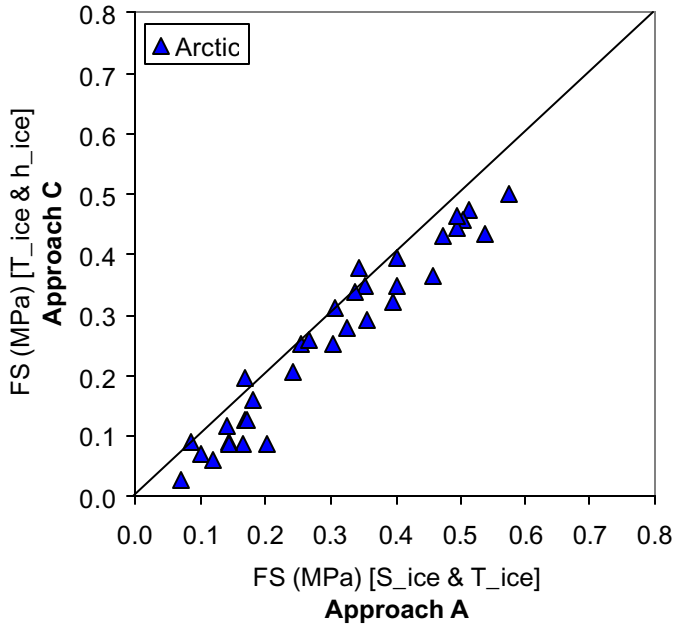

(a) Approach A vs. Approach C

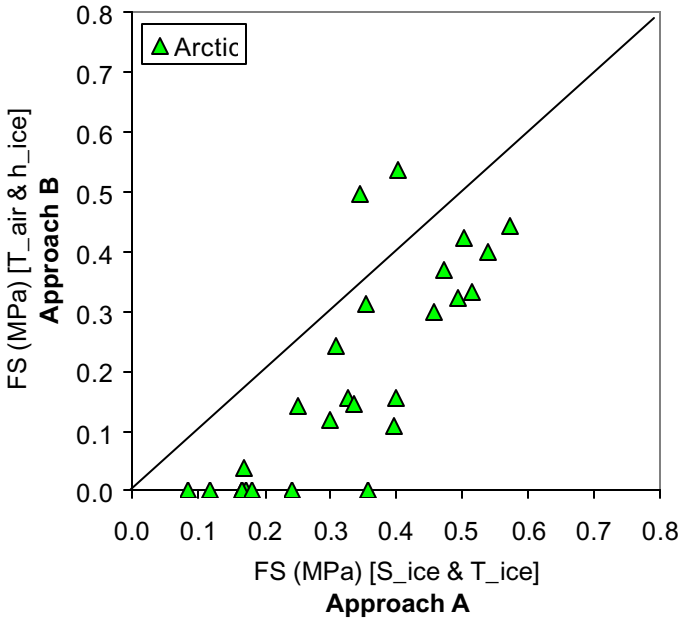

(b) Approach A vs. Approach B

Figure 6 Cross-plots of flexural strength calculated using different approaches

5.0 First-year Ice in the Sub-Arctic: Results from Labrador Fieldwork

Having shown similar trends in the ice borehole strength and the calculated flexural strength of first-year ice in the Arctic, the question arises as to whether a similar relation exists for first-year ice in the sub-Arctic. This is explored in the following sections using results from recently conducted fieldwork on level, landfast first-year ice near Nain, Labrador. After providing information about the general ice conditions, the discussion focuses on the *in situ* ice temperature measurements, since they have direct bearing on the measured and calculated ice strengths.

5.1 Sampling Dates and Air Temperature Records

The CHC undertook a measurement program on level, landfast first-year ice near Nain, Labrador in the winter of 2004. Adequately characterizing the growth and decay of sub-Arctic ice required four trips be made to Labrador during the winter and spring of 2004, the dates of which are shown in Figure 7. The first trip to Labrador extended from 27 January to 4 February (Julian Day, JD27 to JD35) [4]. The second trip was made from 23 March to 29 March (JD83 to JD89) [5]. The third trip was made from 13 April to 20 April (JD104 to JD111). The fourth and final trip to Labrador was made from 11 May to 16 May (JD132 to JD137).

Figure 7 also shows the plot of the hourly air temperatures for Nain, courtesy of Environment Canada. Large temperature fluctuations are characteristic of the area. Take, for instance, late March (Trip 2) when the air temperature dropped 23°C over a 16-hour period (from a temperature of +7°C to -16°C). Radical temperature fluctuations occurred frequently, and were usually accompanied by high winds and mixed precipitation.

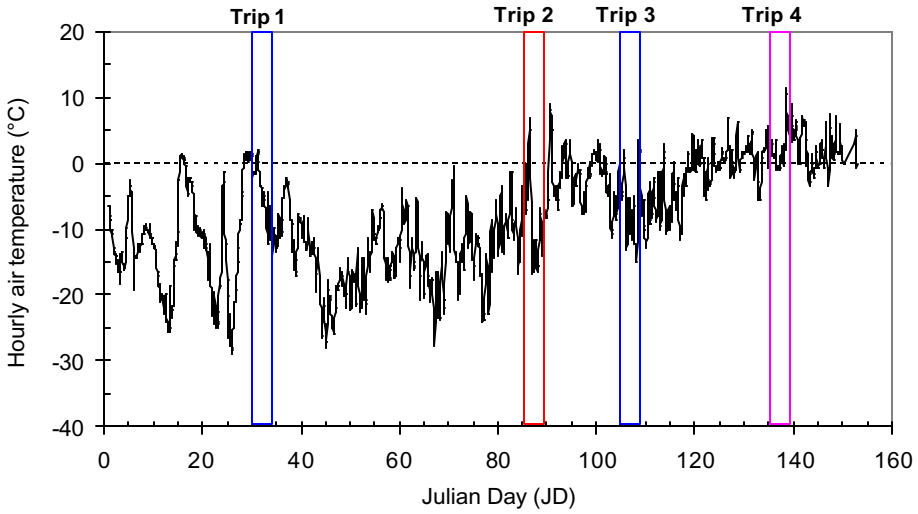

Figure 7 Air temperatures in Nain from January to May, 2004 (data courtesy of Environment Canada)

[4] The dates shown in the figure include the time needed to travel to Nain, from Ottawa.
[5] Note that 2004 was a leap year, which influenced numbering the Julian Days after February.

5.2 Sampling Sites

Figure 8 shows the two transects that were made on level, landfast ice in Strathcona Run and in Anaktalak Run. The level ice in Strathcona Run was chosen because it coincided with the 'traditional' shipping route to Nain, whereas the sampling sites in Anaktalak Run coincided with the proposed shipping route to Voisey's Bay Mine site, at Edward's Cove (Dickens and Dempsey, 2005). Ten sites, each separated by a distance of 1 km, were sampled along the two transects. In February, temperature chains were installed in the ice at Site S7 in Strathcona Run, and Site A1 in Anaktalak Run. Measurements from those two temperature chains will be discussed in a later section.

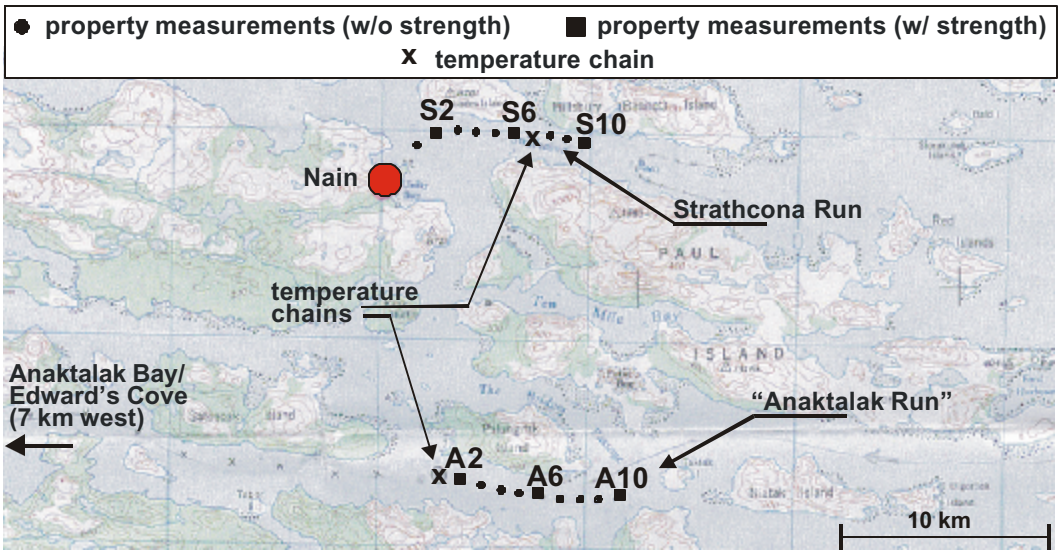

Figure 8 Sampling sites in Strathcona Run ('S'), Anaktalak run ('A')

Table 1 lists the UTM coordinates of the sampling sites, and the property measurements that were made at each site during the different visits. Measurements included the snow thickness (h_s), ice thickness (h_i), ice freeboard (FB), and profiles of the ice salinity (S) and temperature (T) of the extracted cores, and profiles of the *in situ* borehole strength of the ice (σ). Depending upon the time available, different measurements were conducted at different sites. The most complete set of property measurements was made at Sites S2, S6 and S10 (Strathcona Run) and sites A2, A6 and A10 (Anaktalak Run). Johnston (2005) presents a detailed discussion of the measurements made in the level ice, as well as measurements made in April, at four sampling sites in hummocked ice.

Figure 9 plots the measured snow and ice thicknesses at Sites S2, S6 and S10 in Strathcona Run, and Sites A2, A6 and A10 in Anaktalak Run. Data in the figure represent the average of the measurements made in multiple boreholes at the individual sites (see Appendix A). Because the data in Figure 9 represent the three-hole average, they do not show the variable conditions that characterized each of the three boreholes made at any one site. Local variations in snow thickness at Sites S2, S6 and S10 were up to 210 mm, with an ice thickness variation of 105 mm, or less. In Anaktalak Run, the local variations in snow thickness were up to 230 mm, and the maximum variation in ice thickness was 130 mm.

Table 1 Properties Measured on Ice Cores during 2004 Season

Site	UTM coordinates (N, W)	h_s, h_i, FB [a]	S, T [b]	σ[c]
S1	0581682, 6268927	Feb/Mar	Feb	
S2	0582488, 6269484	Feb/Mar/Apr/May	Feb/Mar/Apr/May	Mar/Apr/May
S3	0583473, 6269545	Feb/Mar	Feb	
S4	0584471, 6269626	Feb/Mar	Feb/Mar	03
S5	0585464, 6269658	Feb/Mar	Feb	
S6	0586464, 6269720	Feb/Mar/Apr/May	Feb/Mar/Apr/May	Mar/Apr/May
S7	0587444, 6269770	Feb/Mar	Feb	
S8	0588452, 6269761	Feb/Mar	Feb/Mar	03
S9	0589464, 6269754	Feb/Mar	Feb	
S10	0590452, 6269736	Feb/Mar/Apr/May	Feb/Mar/Apr/May	Mar/Apr/May
A1	0583101, 6253463	Feb/Mar	Feb	
A2	0584030, 6253375	Feb/Mar/Apr/May	Feb/Mar/Apr/May	Mar/Apr/May
A3	0585036, 6253288	Feb/Mar		
A4	0586031, 6253203	Feb/Mar	Feb/Mar	
A5	0587023, 6253140	Feb/Mar		
A6	0588035, 6253023	Feb/Mar/Apr/May	Feb/Mar/Apr/May	Mar/Apr/May
A7	0589031, 6252967	Feb/Mar		
A8	0589994, 6253232	Feb/Mar	Feb/Mar	
A9	0590952, 6253538	Feb/Mar		
A10	0591905, 6253865	Feb/Mar/Apr/May	Feb/Mar/Apr/May	Mar/Apr/May

[a] snow thickness (h_s), ice thickness (h_i) and freeboard (FB)
[b] ice salinity (S) and ice temperature (T)
[c] ice borehole strength (σ)

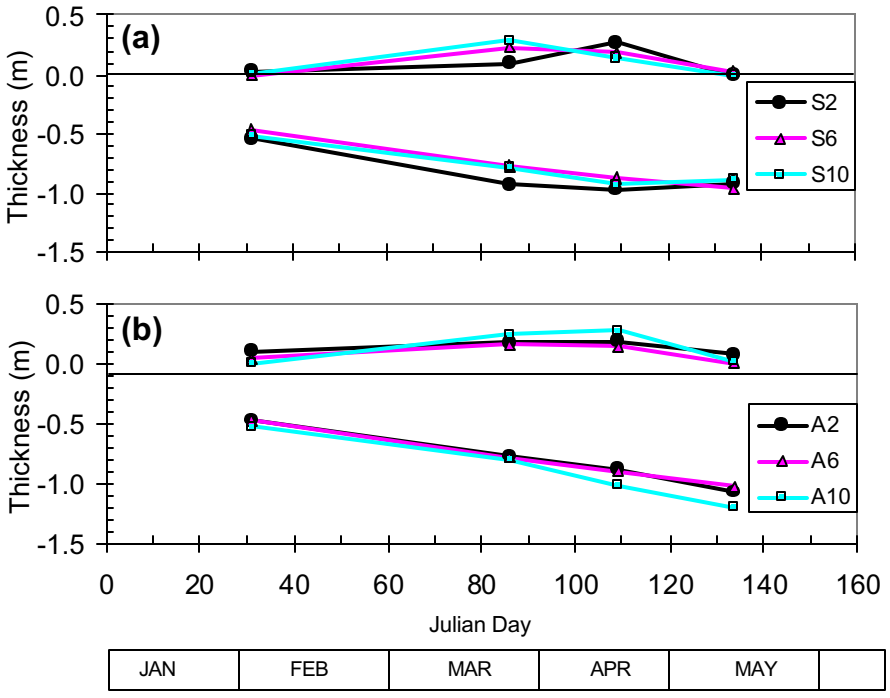

Figure 9 Snow and ice thickness at three sites in (a) Strathcona Run, (b) Anaktalak Run

5.3 In situ Measurements of Air, Snow and Ice Temperatures

One of the primary objectives of the Labrador field program was to obtain a continuous record of the *in situ* temperatures of the air, snow and ice. During the first site visit in late January/early February, one temperature chain was frozen into the level landfast ice at Site S7 in Strathcona Run, and another temperature chain was installed in the level ice at Site A1, in Anaktalak Run (Figure 8). The chains were designed to measure temperatures in the air, snow and ice at 30-minute intervals, from February until mid-May (when both chains were removed).

5.3.1 Temperature Chain at Site S7, Strathcona Run

On the morning of 1 February (JD32), one of the temperature chains was installed in 0.50 m thick ice at Site S7. Site S7 was selected for the installation because it was far enough from the community to avoid interfering with the snowmobile traffic. Figure 10 shows a schematic of the temperature chain that was installed at Site S7. The following gives a brief description of how the temperature chains were constructed. Note that in this report, temperature sensors above the ice surface are shown as "+", and sensors below the top ice surface are shown as "-".

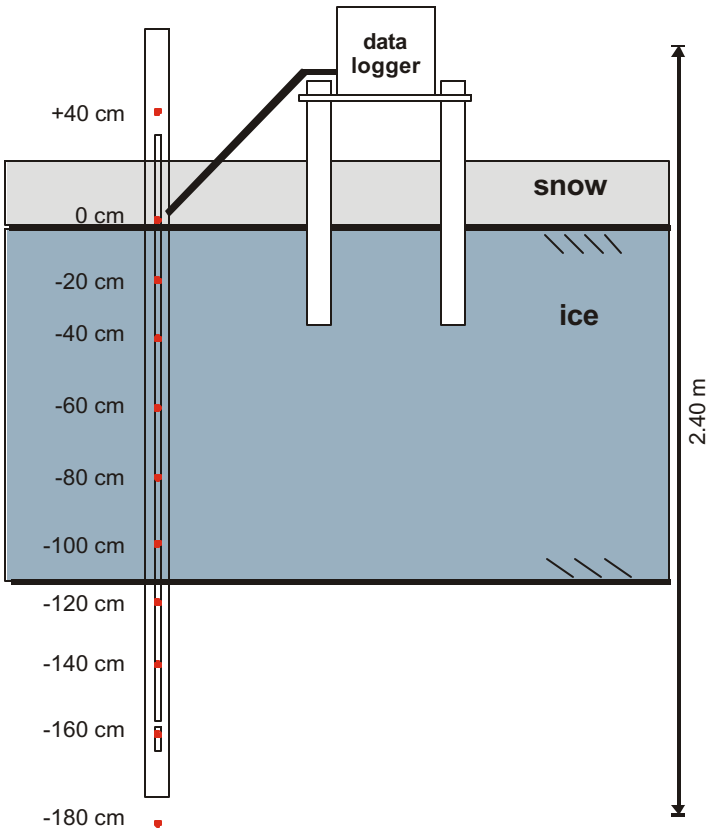

Figure 10 Schematic of temperature chain used at Site S7, Strathcona Run (maximum measured snow and ice thickness shown in illustration)

To minimize potential absorption of solar radiation, the temperature chains were constructed of white PVC pipe, 2.40 m long and 50 mm in diameter. A slot was cut down one side of each PVC pipe so that water was able to penetrate the temperature chain, allowing ice to form around the thermocouple sensors, yet preventing the pipe from splitting as it froze into the ice. The thermocouple wires extended from the data logger, down the inside of the PVC pipe, where they exited into the ice through small holes in the pipe. By design, each sensor extended about 10 mm from the pipe to minimize the effect of preferential melting that might occur around the temperature chain. All of the thermocouple wires were covered with white electrical tape. The sensor tips were covered with waterproof, white heat shrink.

At Site S7, the temperature chain was installed so that the sensor at a depth of 0.0 m was flush with the top ice surface. To prevent the chain from moving before it froze in place, a horizontal bar was slipped through small holes that had been made in the chain at depth 0.0 m, and the ends of the bar were weighted down with packed snow. The uppermost sensor, which was located +0.40 m above the ice surface (the maximum snow thickness expected for that area) measured air temperatures at the site. The sensor at 0.0 m measured the ice surface temperature. Below the ice surface, the sensor spacing was 200 mm, to a depth of -1.80 m. Although the mean thickness of level ice in that area[6] does not usually exceed 1.10 m, the sensors extended to a depth of 1.80 m because that chain was meant to be installed in thicker, ridged ice. Since there was no rough ice in February, when the chains were installed, the level ice at Site S7 was used instead.

Once the temperature chain had been properly installed, the thermocouple wires were connected to the data logger (Figure 11-a). Data loggers for the temperature chains were suspended on platforms, the legs of which were frozen into the ice (Figure 11-b). The platforms were placed as far away from the temperature chain as possible, to prevent preferential melting around the chain. The next day, 2 February, the temperature chain at Site S7 was re-visited to verify that it was functioning properly. Figure 11-b shows the temperature chain after its installation. The first measurements from the temperature chain were recorded at 12:00 hours on JD32.

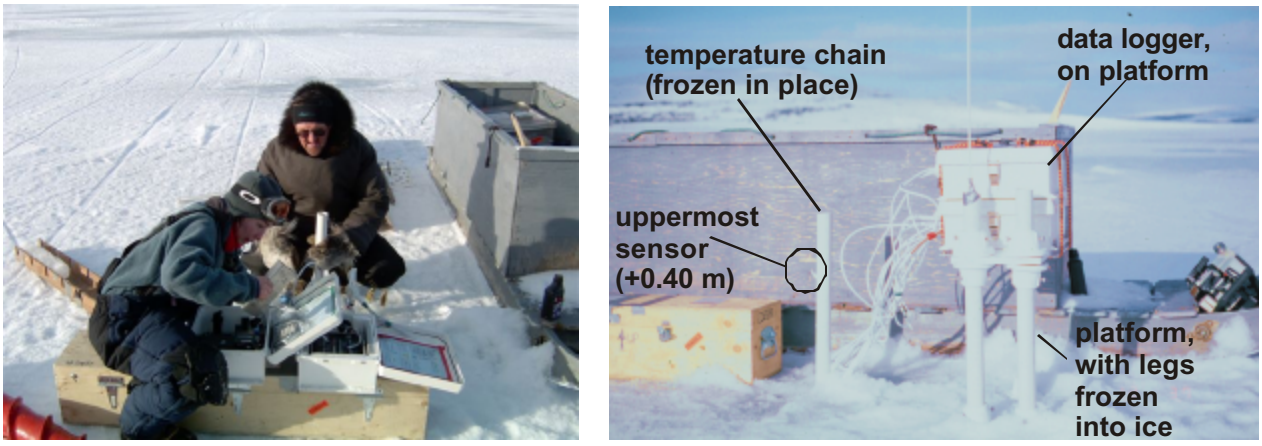

(a) wiring thermocouple connections **(b) chain and platform, frozen in place**

Figure 11 Installing the temperature chain at Site S7, 1 February

[6] ice thickness measurements for Hopedale, Labrador (a coastal community 150 km south of Nain) were available from 1959 to 1983, courtesy of Environment Canada.

5.3.2 Temperature Chain at Site A1, Anaktalak Run

On 2 February (JD33), the second temperature chain was installed in 0.44 m thick ice at Site A1, in Anaktalak Run (Figure 8). Figure 12 shows that the 2.40 m long chain was equipped with more sensors than the chain at Site S7. Its uppermost sensor was located +0.70 m above the ice surface, to ensure that air temperatures were measured throughout the season. The sensor at a depth of 0.0 m was flush with the ice surface. Sensors below the ice surface were spaced at 100 mm intervals, to a depth of -0.30 m. A sensor spacing of 200 mm was used below that depth, until the last sensor was reached, at a depth of -1.10 m. The first measurements from the temperature chain at Site A1 were recorded on JD33 at 11:30 hours.

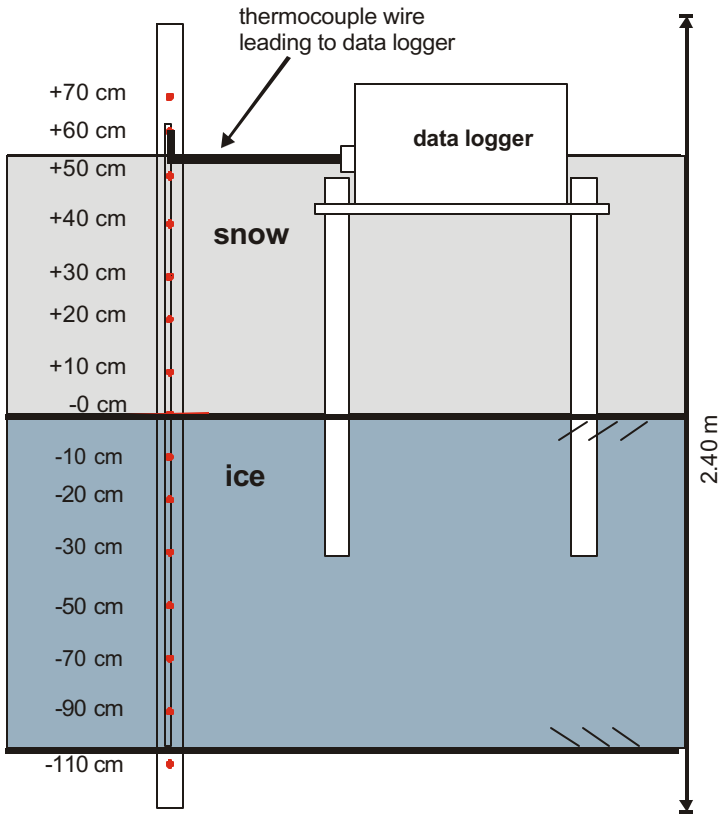

Figure 12 Schematic of temperature chain at Site A1, Anaktalak Run (maximum measured snow and ice thickness given in illustration)

Data from the seven above-the-ice sensors could be used to compare the (different) slopes of the temperature profiles in air, snow and ice. By providing information about the position of the different interfaces (air/snow and snow/ice), changes in the snow cover could be related to the effect changing air temperatures had on the underlying ice cover. The sensor at a height of +0.70 m also provided measurements of the air temperature, should a substantial amount of superimposed ice form on the top ice surface. Superimposed ice can comprise a significant part of the ice cover in Labrador, since that area experiences heavy snowfall, which can depress the ice cover, flood the snow cover and freeze, causing ice to form.

Figure 13 shows the temperature chain at Site A1 during the four site visits to Labrador. In February, all seven above-the-ice sensors were exposed to the air. In March, the sensor at a height of +0.10 m was barely in contact with the snow (Figure 13-b). Very different conditions were encountered in April, when snow covered the sensors to a height of +0.50 m (Figure 13-c). When the temperature chain was removed on 13 May, the snow cover extended to the +0.40 m sensor (Figure 13-d).

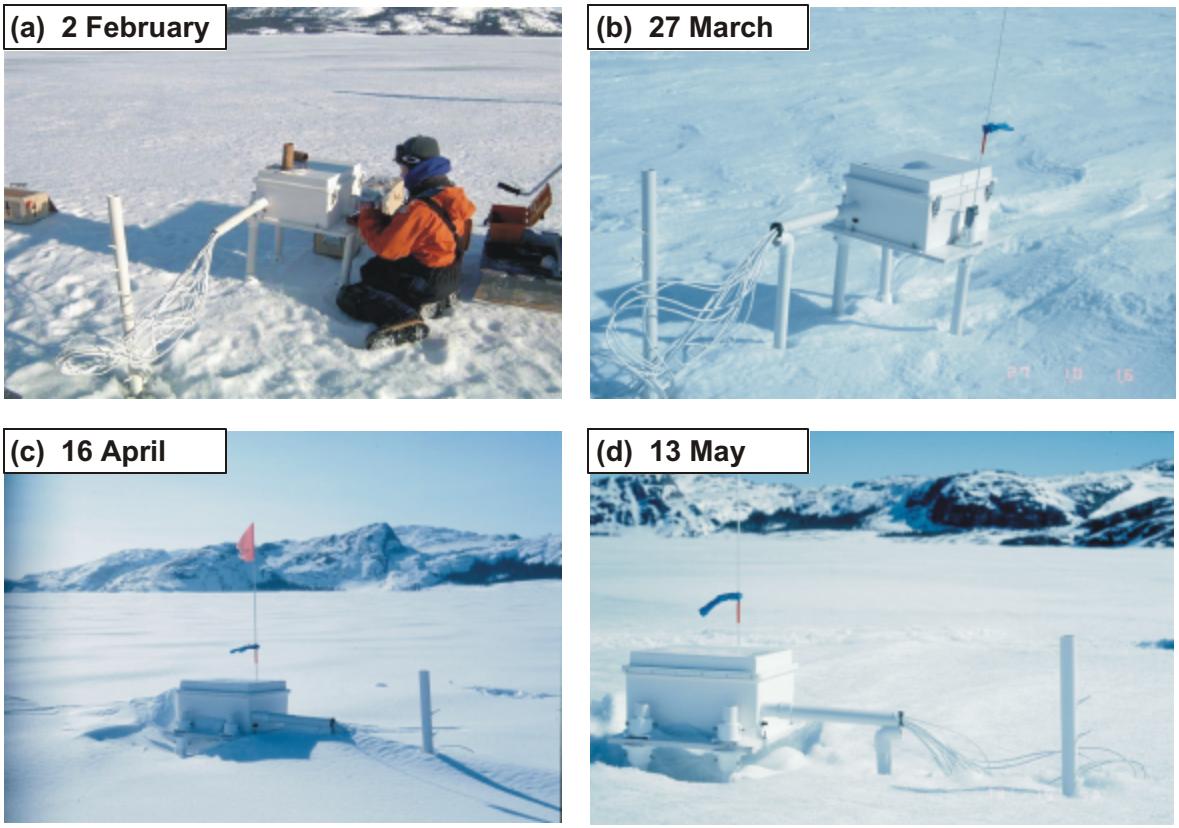

Figure 13 Temperature chain at Site A1, from February to May

5.3.3 Air Temperatures: *In situ* vs. Environment Canada

Air temperatures at each site can be determined from the uppermost sensors of the temperature chains (+0.40 m at Site S7 and +0.70 m at Site A1), because those sensors remained above the snow cover throughout the season. That was verified by comparing data from the uppermost sensors to air temperatures measured by Environment Canada's (coastal) automatic weather station in Nain[7]. Figure 14 shows that the uppermost sensor in both chains measured temperatures that were in good agreement with the air temperatures reported by Environment Canada. Temperatures measured on the ice were somewhat colder than those reported by Environment Canada, however.

[7] Environment Canada lists two stations for Nain. Data were obtained for the Nain weather station with the WMO identifier 71665, elevation 6.7 m (rather than the Nain station with an elevation of 7.6 m).

Installing temperature chains at two locations, about 35 km apart, provided a means of quantifying variability in regional air temperatures. The histogram in Figure 15 shows temperature measurements for the two sites, from February 3 to May 13, at 30-minutes intervals. Positive temperature differences indicate that the air temperature at Site A1 was colder than Site S7. Negative temperature differences indicate that air temperatures at Site A1 were warmer than Site S7. Air temperatures at the two sites were usually within ±1°C of each other (shown by the black column), although temperatures at Site A1 were sometimes colder than Site S7 (by up to 11°C, as shown by the green columns). Less frequently, temperatures at Site A1 were warmer than Site S7, by as much as 5°C.

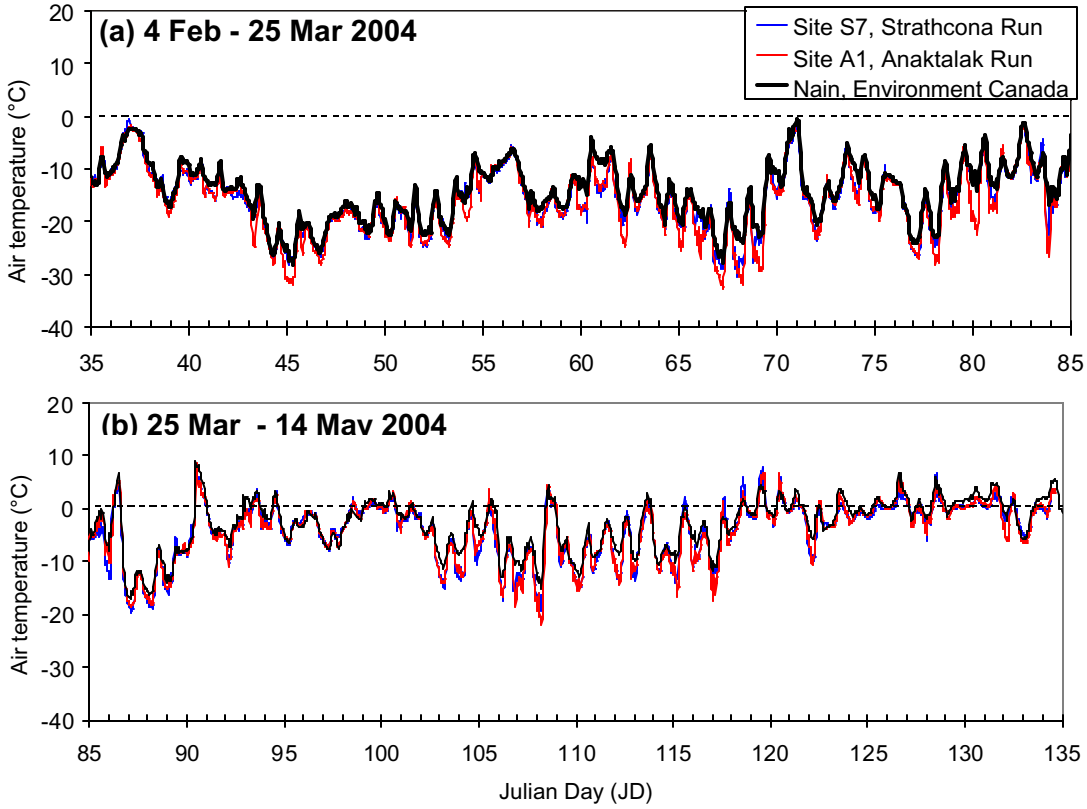

Figure 14 Comparison of air temperatures at different sites

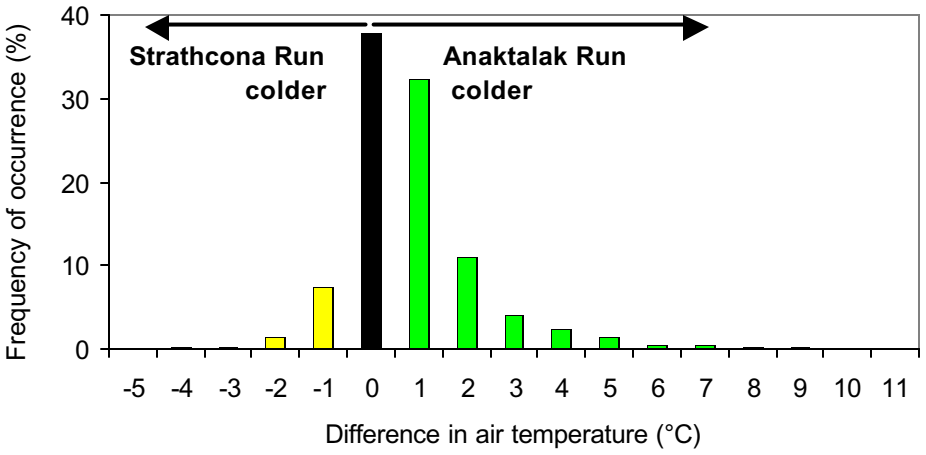

Figure 15 Air temperature difference at Site S7 and Site A1
(measurements from sensor at +0.40 m shown for Site S7, and +0.70 m for Site A1)

5.3.4 *In Situ* Ice Temperatures at Two Locations

Figure 16 compares the *in situ* temperature profiles at Site S7 and Site A1 for seven days, spanning 5 February (JD36) to 13 May (JD134). The temperatures in the figure were reported at 06:00 hours when, after a cold night, the conditions were more stable than later in the day. A solid data marker was used to show the location of the top ice surface (0.0 m) when the temperature chains were installed. Dotted lines were used in Figure 16 to show the approximate height of the air/snow interface at Site A1, gauging from the different slopes that characterized sections of the temperature profile. Table 2 shows that the snow thicknesses measured at Site A1 were in good agreement with the location of the air/snow interface that was inferred from the temperature profiles in Figure 16.

February

Figure 16-a shows that on 4 February (JD35), Site S7 and Site A1 had equivalent air temperatures (-9.4°C), yet the top surface of ice at Site S7 was several degrees colder than at Site A1 (-8.5°C vs. -5.9°C). Temperatures at a depth of -0.20 m were also colder at Site S7 than Site A1 (-5.2°C vs. -2.0°C). The difference in the ice temperature profiles likely resulted from the ice at Site S7 being thicker than at Site A1 (Table 2). In February, the ice thickness at Site S7 ranged from 0.49 to 0.50 m, and the snow was from 40 to 70 mm thick. The ice thickness in two boreholes at Site A1 was 0.46 and 0.41 m, and the snow thickness was 0 and 80 mm.

March

On 25 March (JD85), the ice at both sites was considerably colder than in February (Figure 16-c). The air temperature at Site S7 and Site A1 was -5.5°C, and -5.3°, respectively. Temperatures at the ice surface and at a depth of -0.20 m were similar at Site S7 and Site A1 (respectively -6.5°C and -6.2°C at the top ice surface, and -5.6°C and -5.2°C at a depth of 0.20 m). The ice at Site S7 was 0.81 m thick and had 150 to 200 mm of snow, whereas the ice at Site A1 was 0.71 m thick and had a 110 to 240 mm deep snow cover (Table 2).

Table 2 Ice and Snow Thicknesses around Temperature Chains
(measurements made in one to three boreholes

Date	Julian Day	Site S7		Site A1	
		h_i (m) [a]	h_s (mm) [b]	h_i (m)	h_s (mm)
1 Feb	JD32	0.50, 0.49, 0.50	70, 50, 40		
2 Feb	JD34			0.46, 0.41	0, 80
25 Mar	JD85	0.81, 0.81[c]	200, 150 [c]		
27 Mar	JD87			0.71, 0.71	240, 110
16 Apr	JD107			0.83, 0.92, 0.90	260, 280, 240
17 Apr	JD108	0.85, 0.90, 0.87 [c]	200, 180, 150 [c]		
13 May	JD134	1.17	10	1.04	140

[a] ice thickness
[b] snow thickness
[c] measurements made at Site S6

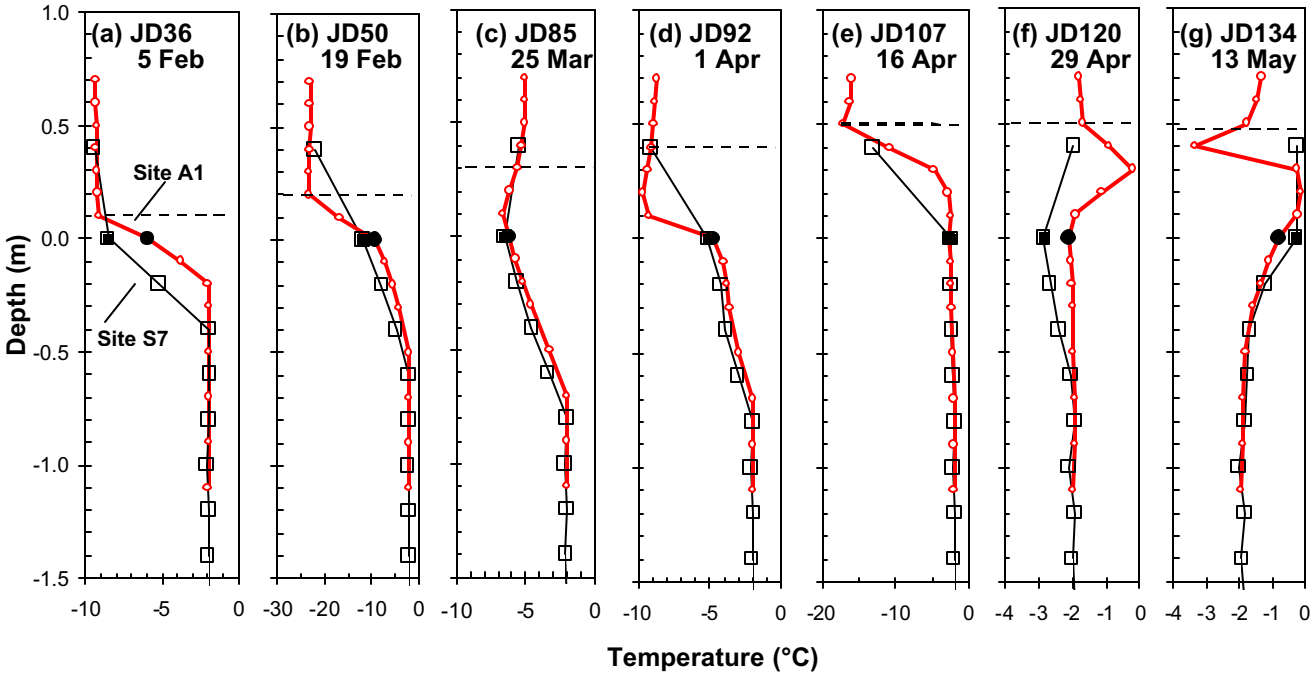

Figure 16 Comparison of *in situ* ice temperatures at Site S7 and Site A1
(black data markers indicate top ice surface when chains were installed; dotted line shows approximate air/snow interface at Site A1, gauging from slope of data; note the temperature scale varies for the different plots)

April

Air temperatures on 1 April and 16 April were cold (about -9.0°C and -12°C respectively), even though the average air temperature during the first two weeks of April was just -3.0°C (Figure 14). Between 1 April and 16 April, the ice temperature profile at both sites changed considerably. On 1 April (Figure 16-d) the ice temperature profiles were linear, where the top ice surface was colder than the bottom surface. However on 16 April (Figure 16-e), the ice was isothermal, and had a temperature of -2.4°C throughout its full thickness. The two weeks of warm air temperatures that occurred in early April clearly affected the ice at both sites.

On 29 April (JD120) the air temperature was -2.0°C at Site S7 and -0.9°C Site A1 (Figure 16-f). It is interesting to note that while the ice at Site A1 was isothermal in late April, the ice at Site S7 was characterized by a linear temperature profile, where the top ice surface was colder than the bottom ice surface. Temperatures in the surface layer of ice at Site S7 were -2.8°C and -2.7°C (for depths of 0.0 m and -0.20 m), whereas the surface layer of ice at Site A1 was slightly warmer (-2.1°C and -2.0°C at 0.0 m and -0.20 m respectively). The different profiles may have resulted from the snow cover being thicker at Site A1, or because a thicker layer of superimposed ice may have formed at Site A1.

The temperature profile for Site A1 in Figure 16-f shows evidence of three distinct regions, each of which is marked by an inflection point (+0.50 m, +0.30 m and 0.0 m). The inflection point at +0.50 m likely corresponded to the air/snow interface. The inflection point at 0.0 m coincided with the "original" top ice surface, below which congelation ice extended (and was uniformly isothermal). The reason for the inflection point at +0.30 m is not clear, although it may indicate that a layer of superimposed ice formed above the original top ice surface. Because the air, snow, superimposed ice and congelation ice each have different thermal properties, the temperature profile differs for each medium.

May

By 13 May (JD134), the snow cover at Site S7 had melted almost completely, leaving a thin crust of snow-ice on the ice surface. In comparison, the ice at Site A1 was covered by a 140 mm of snow. When the temperature chain was removed on 13 May only the uppermost three sensors were exposed at Site A1 (Figure 13-d).

Figure 16-g shows that by mid-May, the full thickness of ice at Site S7 (1.17 m) and Site A1 (1.04 m) were characterized by isothermal, near-melting temperatures. Analysis showed that the temperature of -3.4°C at +0.40 m resulted from the cold air temperatures on the mornings of JD132 and JD133. Air temperatures warmed on JD134. The temperature profile shows that the snow above and below the sensor at +0.40 m responded more quickly to the warm air temperatures than the sensor at the +0.40 m height. The thin layer of snow (or superimposed ice) around +0.40 m still showed an effect from cold air temperatures of the previous two days (not shown).

5.3.5 Ice Temperatures: Extracted Cores vs. *In Situ* Measurements

Part of the field measurements on decaying ice in the high Arctic and the sub-Arctic relied upon measuring the temperature of the extracted ice core (see Appendix A). Because that technique has been an integral part of the measurement program over the years, the next section examines the accuracy with which temperature measurements can be made on the cores.

Figure 17 shows the comparison of temperatures measured on the extracted ice cores and those measured from the *in situ* temperature chains at Site S7 and Site A1, during each of the four trips to Labrador. Because ice cores were not usually extracted from either Site S7 or Site A1, the figure shows temperatures of the cores extracted at the closest site. The profiles show that temperatures measured on the extracted ice cores were higher (by as much as +2°C) than the *in situ* measurements from the temperature chains. Note that on occasion, measurements on the extracted ice core were higher than 0°C, which attests to the limited accuracy of the temperature probe when the air temperatures are above 0°C, or ice temperatures are near melting. The temperature chain, by comparison, consistently measured subzero ice temperatures, except when sensors were not covered by ice (when the sensors at the top ice surface were exposed, they registered temperatures above 0°C).

The figure shows that measuring temperatures on extracted ice cores is relatively accurate when the ice is cold, however there are inaccuracies when the ice is warm (in fall or spring). Although measuring the temperature of the core provides an indication of the relative changes in the shape of the temperature profile, it is not effective for measuring absolute ice temperatures. Errors in the technique arise because the temperature probe has limited accuracy (±2°C) when the ice is at near-melting temperatures, and also because the properties of the ice change soon after the core has been removed from the ice.

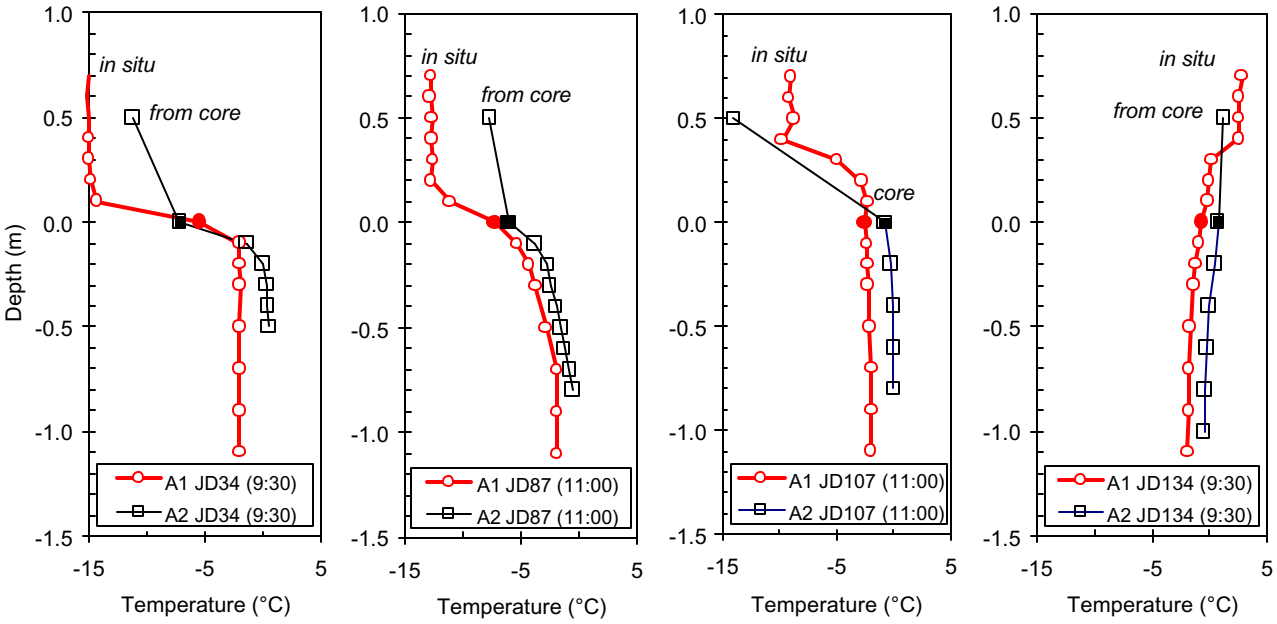

(a) Strathcona Run

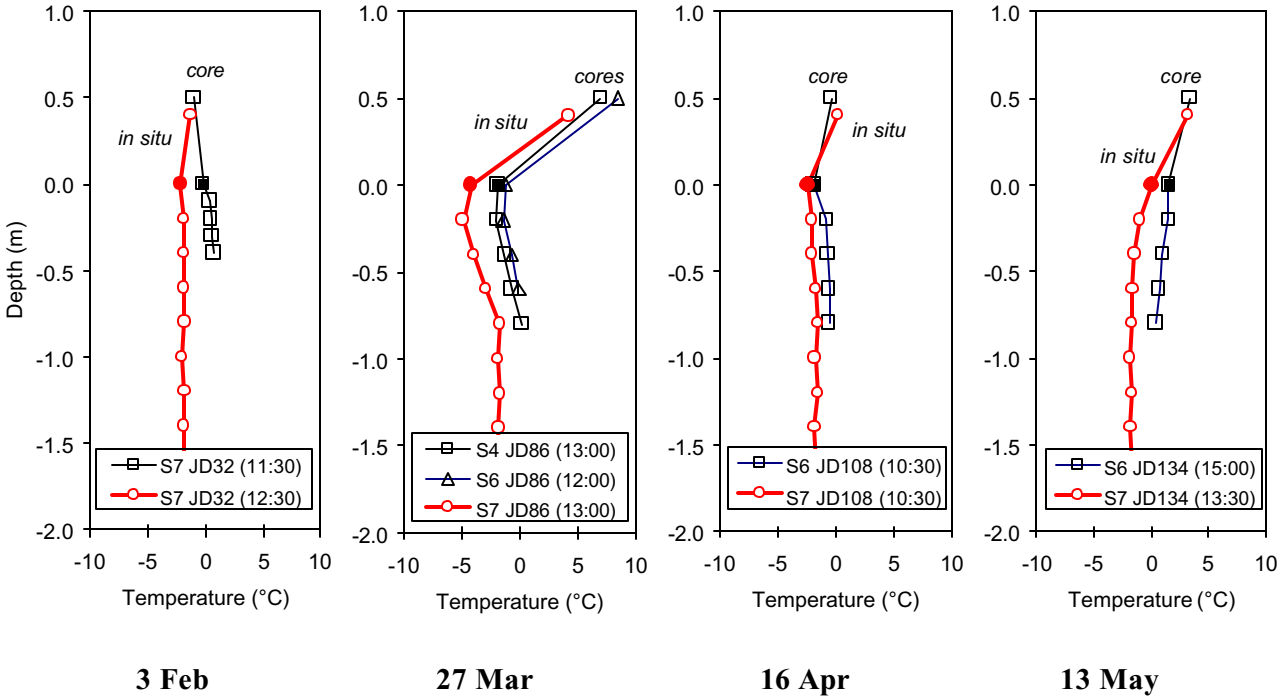

(b) Anaktalak Run

Figure 17 Temperatures of extracted ice cores vs. *in situ* measurements (solid data markers show top ice surface when chain was installed)

6.0 Strength of Sub-Arctic Ice

Property measurements made in first-year ice near Nain were used in Figure 18 to plot the ice borehole strength and the flexural strength, calculated using Approach A (the measured bulk ice temperature and measured bulk ice salinity). During the first site visit, in late-January/early February (JD33), borehole strength tests were not conducted because only one test (at depth 0.30 m) could have been performed in the 0.50 m thick ice. In addition, edge effects from the top and bottom ice surfaces would likely have affected tests at that depth.

Some of the lowest calculated flexural strengths occurred in February (JD33), when the ice was still quite thin and warm. The highest strengths were measured (and calculated) in March (JD88). From March to May (JD134) the measured ice borehole strength decreased. The calculated flexural strength also decreased from March to April (JD108), yet unlike the measured strength, the calculated flexural strength *increased* in May, compared to the previous site visit.

Two factors were used to show that the late-season increase in the calculated strength was an artifact. First, the ice borehole strength continued to decrease as the season advanced, a trend that has also been observed in Arctic first-year sea ice (Figure 3). Second, as the ice decayed, the bulk temperature of the ice at Site S7 and Site A1 increased and its salinity decreased. The warming and desalination of the ice sheet are clear signs of its weakened state, however Approach A interpreted the decreased ice salinity as a "freshening" of the ice, which resulted in an increase in strength.

In fact, the flexural strength should have decreased in mid-May, because the total porosity of the ice (air and brine pockets) increases during the decay process. The deteriorated state of the cores was clearly evident during the May site visit, as discussed in Johnston (2005). As the ice warms, brine pockets increase in size and eventually interconnect to form "highways" that facilitate brine drainage. Because the ice salinity decreases as the ice decays, the brine will decrease, however the enlarged brine drainage channels cause an increase in the total porosity of the ice. It is the increase in total porosity that causes the ice strength to decrease, as shown by the *in situ* borehole strength tests in the high Arctic, and in Labrador.

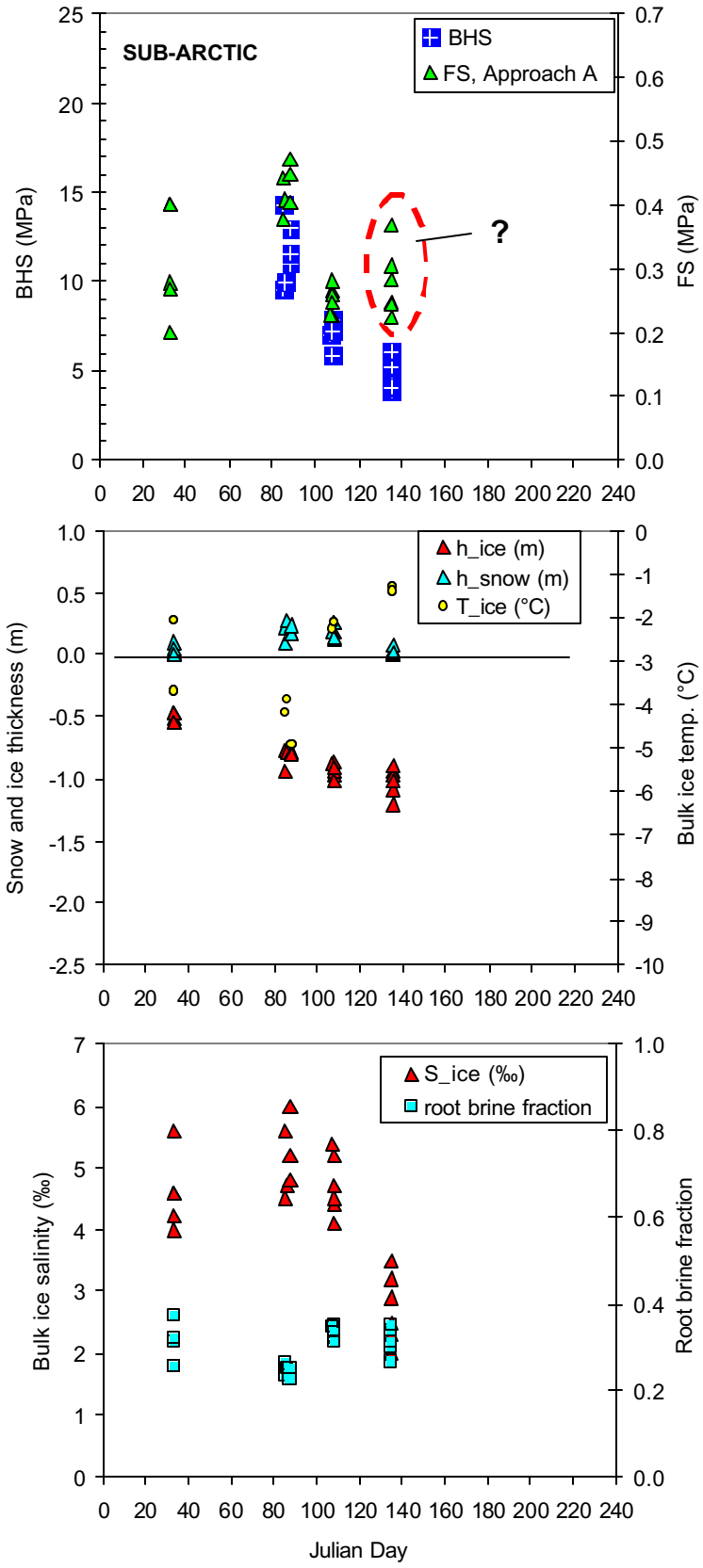

Figure 18 Comparison of two techniques for calculating flexural strength

6.1 Compensating for the Increased Total Porosity of the Ice, Late in the Season

Because there are so few accurate measurements of ice density available, the effect of total porosity on ice strength was not able to taken into account in Equation (1), which is why the calculated flexural strength increases late in the season. It would be possible to modify the flexural strength equation to account for the total porosity of the ice, if accurate measurements of the ice density were available. They are not. An alternate way of accounting for the increase in total porosity of the ice, late in the season, would be to hold the ice salinity constant after a certain date, while taking into account the increase in the measured ice temperature. In effect, that would produce an apparent increase in brine volume, as a substitute for the actual increase in total porosity.

Figure 19 shows the results of that technique, whereby the bulk salinity of the ice from April (JD108) was used to calculate the flexural strength in May (JD134). That technique corrects for the erroneous increase in flexural strength (shown in Figure 18), which allows the calculated flexural strength to fall in line with the measured borehole strength.

It should be noted that allowing the ice salinity to decrease (as measured), and holding the ice temperature constant does NOT produce the same result. Clearly, the brine volume is a stronger function of the salinity, than the ice temperature.

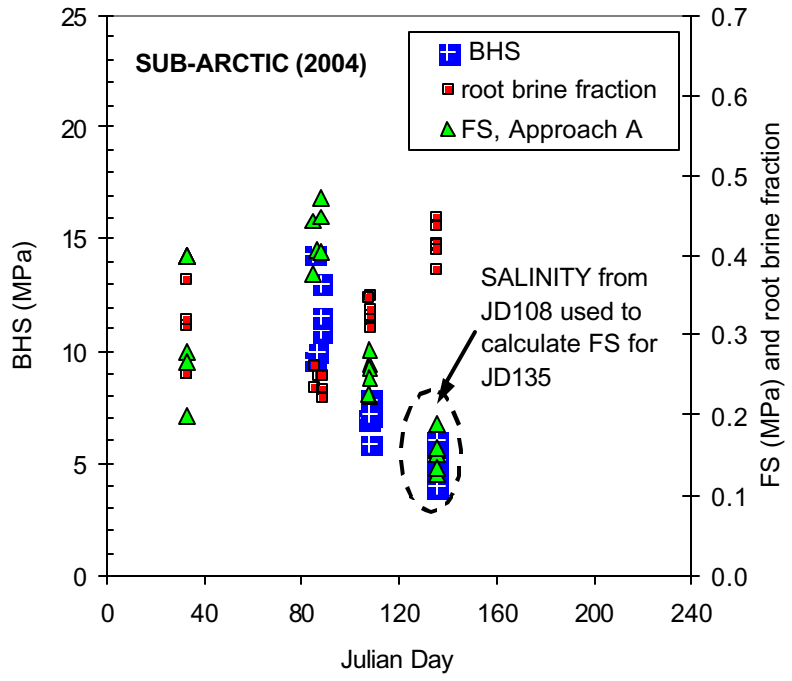

Figure 19 Technique for extending Approach A to late season sub-Arctic ice

7.0 Determining Bulk Ice Temperature from Air Temperatures

The previous discussion showed the importance of having accurate measurements with which to calculate the flexural strength of the ice. Although Approach A is preferred for calculating the flexural strength, it was shown that Approach C can also be used with reasonable success, provided the bulk ice temperature is known. Since it is not possible (or desirable) to measure the *in situ* temperature of the ice at stations throughout the Arctic and sub-Arctic, the logical next step would be to use the air temperature to determine changes in the ice temperature: the air temperature is the driving force that causes seasonal changes in the ice cover. This section uses *in situ* ice temperatures measured in the sub-Arctic and the high Arctic to explore the relation between the ice temperature and the air temperature.

7.1 Temperatures in the Top Surface of Ice: Sub-Arctic

Figure 20 shows the *in situ* temperature measurements made at Site S7 in Strathcona Run, and Site A1 in Anaktalak Run, Labrador. In both figures, measurements were made at 30-minute intervals. At Site S7, data were plotted from the sensors at depths +0.40, 0.0, -0.20, -0.40 and -0.60 m (Figure 20-a). The uppermost sensor (+0.40 m) was used to provide an indication of the air temperature at that site. Data at Site A1 were plotted for the sensors at +0.70, 0.0, -0.10, -0.20, -0.30, and -0.50 m. The uppermost sensor (+0.70 m) measured air temperatures at Site A1 (Figure 20-b).

Both figures show that daily changes in the air temperature were increasingly attenuated as the ice interior was approached. The top ice surface (0.0 m) responded to short-term fluctuations in temperature, whereas the ice at depths 0.50 m and 0.60 m responded to the longer-term changes in air temperature.

Temperature measurements from both Site S7 and Site A1 can be used to illustrate the effect that snow cover has on transmitting air temperature changes to the ice cover. Take, for instance, the decrease in air temperature that occurred between JD33 and JD37 at both Site S7 and Site A1. The top ice surface (0.0 m) at Site S7 responded immediately to changes in the air temperature that occurred during that period, as did the ice at Site A1. The snow thickness at Site S7 ranged from 0 to 70 mm (Figure 11-a), and from 0 to 80 mm at Site A1 (Figure 13-a) during that time. Another decrease in air temperature occurred at Site S7 and Site A1 from JD37 to JD56. Those changes produced an immediate response in the top ice at Site S7, however the top ice surface at Site A1 showed a delayed response (by about 8 days). The ice at the two sites responded differently, because they may have had different snow thicknesses. That cannot be confirmed, however, since the snow thickness was not measured during that period.

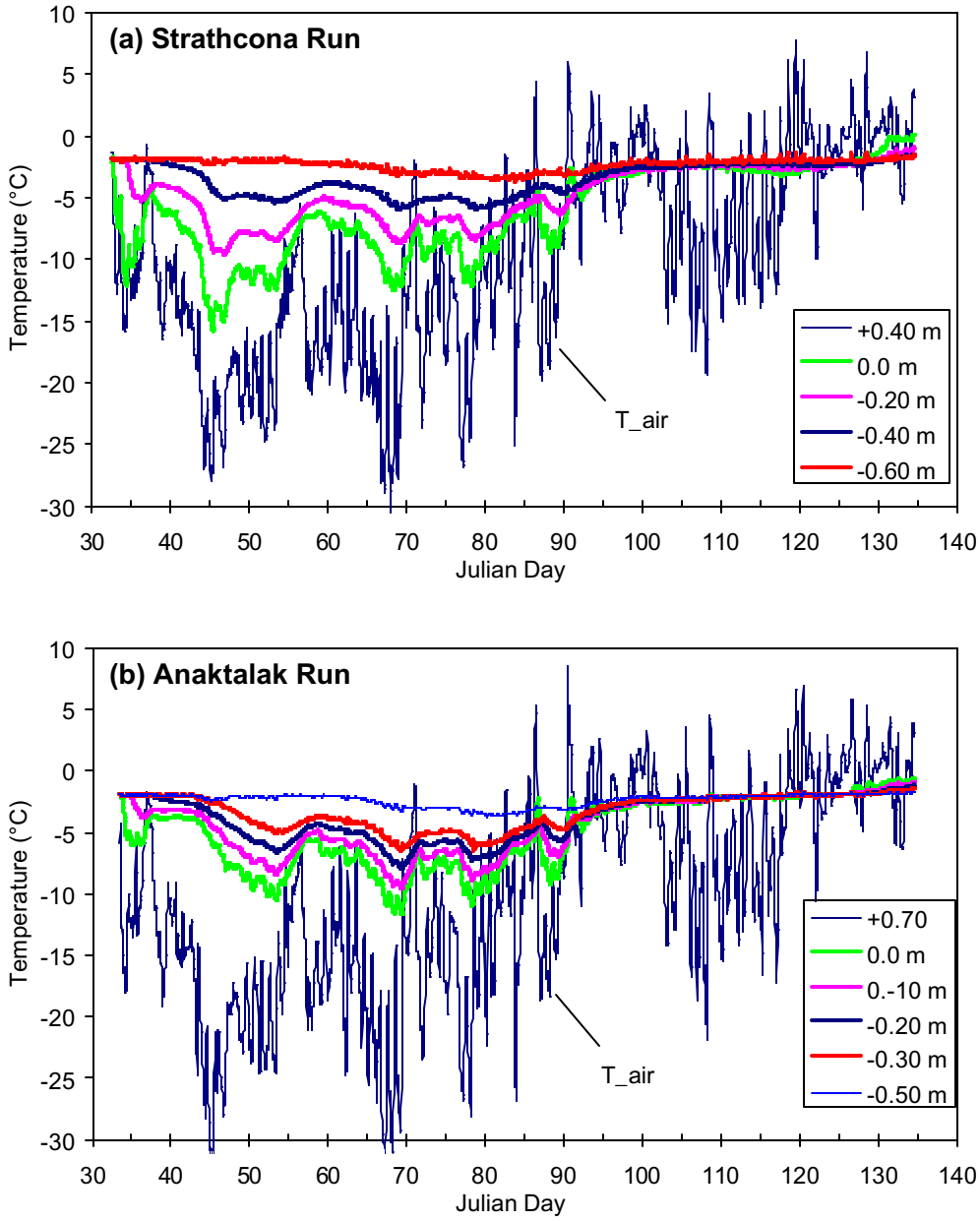

Figure 20 Air and ice temperatures at (a) Site S7 and (b) Site A1

7.2 Relating Bulk Ice Temperature to Air Temperature: Sub-Arctic

Figure 21 shows the bulk ice temperature for Site S7 and Site A1 in relation to the air temperatures at those two sites (sampled every 30 minutes). A 3.5-day moving average was superimposed on the air temperatures for each site. A period of 3.5 days was used because it best reflected trends in the measured bulk temperature of the ice.

The 3.5 day smoothed air temperatures provide a good representation of the trends in the bulk ice temperature at Site S7, from early February (JD36) to about early April (JD94). The 3.5-day moving average also captured the trend in the bulk ice temperature at Site A1. After early April (JD95), the bulk temperature of the ice at both sites was about -3.0°C, and it continued to increase gradually. At that point, air temperature fluctuations had little effect on the bulk ice temperature. For example, both Site S7 and Site A1 experienced a decrease in air temperatures from JD100 to JD120, yet those changes had minimal influence on the bulk ice temperature.

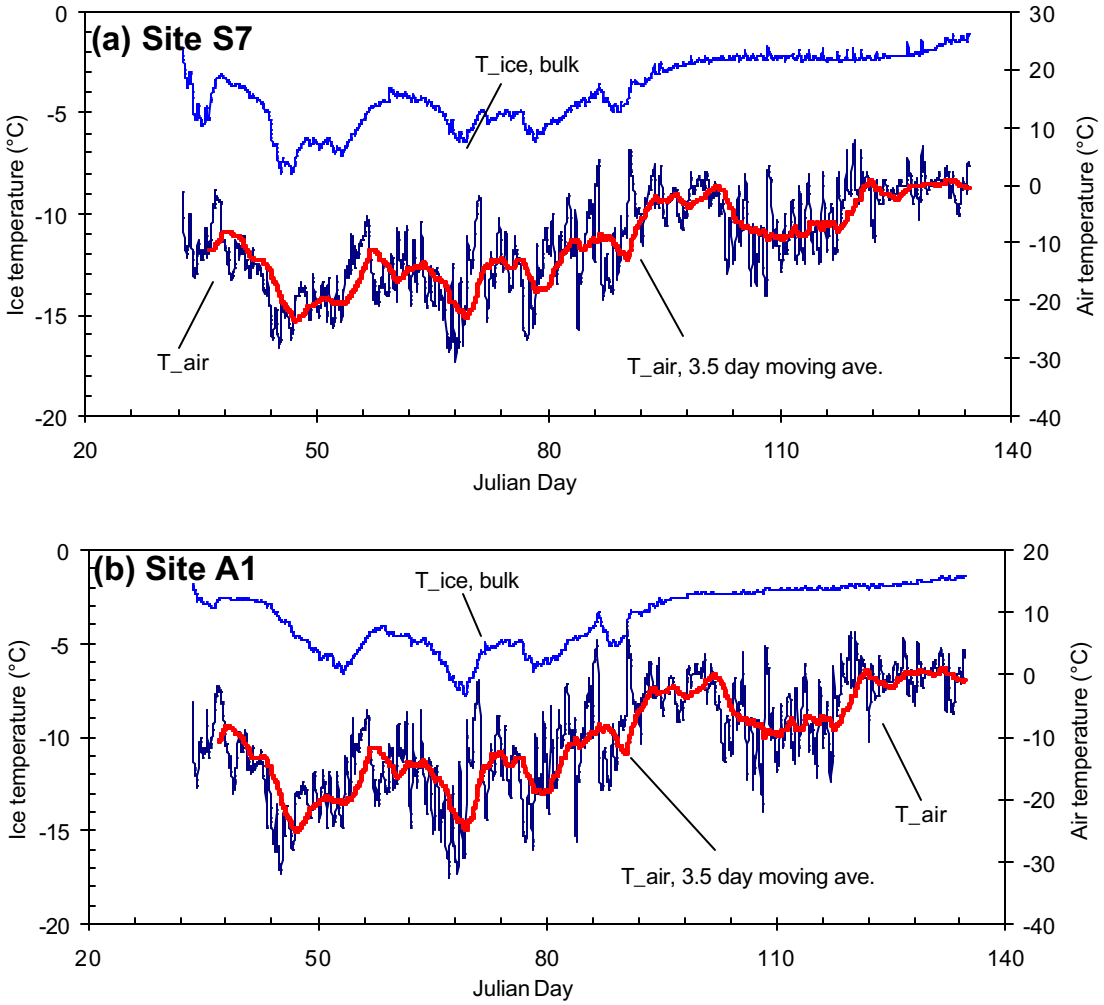

Figure 21 Bulk ice temperature at (a) Site S7 and (b) Site A1

Figure 21 shows one main difference between the ice at Site S7 and Site A1: from JD37 to about JD61, the 3.5 day moving average of the air temperature better represented changes in the bulk ice temperature at Site S7 than Site A1. Notice that the minimum air temperature that occurred on JD47 did not register on the bulk ice temperature until JD53 (6 days later). As stated earlier, that difference is expected to be a result of the different snow thicknesses at the two sites.

7.3 Relating Bulk Ice Temperature to Air Temperature: Arctic

The previous section examined how best to represent changes in the bulk temperature of sub-Arctic ice using air temperature data. A similar investigation was done for first-year ice in the high Arctic, using *in situ* temperature measurements obtained from the temperature chain that CHC installed at Truro Island (75°13.9' N, 97°09.3' W). When the temperature chain was installed on 6 May 2002, the first-year ice at Truro Island was 1.44 m thick and had a 100 mm thick snow cover. When the chain was removed on 5 July 2002, the ice thickness was just over one metre, and a melt pond surrounded the temperature chain. The temperature chain was still frozen solidly in place when it was removed on 5 July, although the ice around the chain had melted by about 0.30 m. Johnston and Timco (2002) provide a detailed description of the ice temperatures measured that season.

Because the first-year ice in the high Arctic typically attains a thickness of 1.8 m or more, sensors along the full length of the temperature chain were used to measure the ice temperature only -- the temperature chain did not measure the air temperatures at Truro Island. Instead, the hourly air temperatures for Resolute (74.72° N, 94.99°W), Environment Canada's closest weather station, were used for the 2002 season. Resolute is about 100 km southeast of Truro Island.

Figure 22 compares *in situ* ice temperatures at Truro Island to the hourly air temperatures for Resolute. The 10-day moving average of air temperature was used in the figure (as a first approach) to establish a relation between the bulk ice temperature and the air temperature. It is interesting to note that the thinner, first-year ice near Labrador (maximum ice thickness of 1.20 m in 2004) was best described by a 3.5 day moving average of the air temperature, yet the thicker first-year ice in the high Arctic (maximum ice thickness of 1.55 m at Truro in 2002) was better described by a 10-day moving average. First-year ice in the Arctic was less responsive to short term variations in the air temperature than ice in the sub-Arctic.

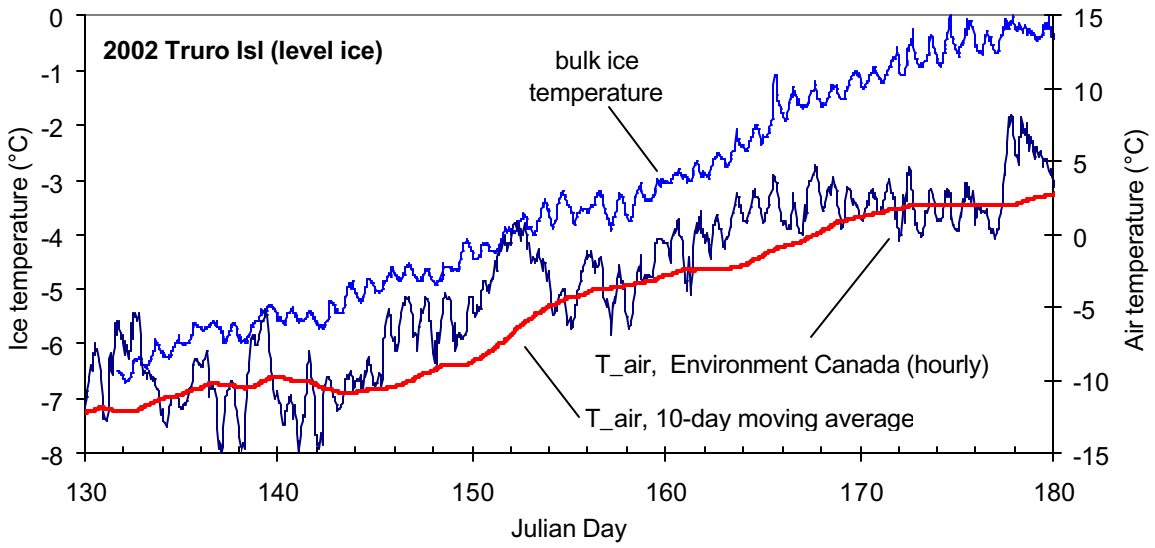

Figure 22 Bulk ice temperature of level first-year ice at Truro Island, high Arctic

7.4 Using Air Temperatures to Estimate the Bulk Ice Temperature

Having shown that the trends in air temperature can be used to represent changes in the bulk temperature of the ice, a first attempt was made to estimate the bulk ice temperature from the measured air temperatures. Figure 23 shows the results of that examination. For the first-year ice in the sub-Arctic, the 3.5-day moving average of air temperature was superimposed on the bulk ice temperature, and an "attenuation" factor of 3.2 was applied to the air temperature data until it showed optimal agreement with trends in the bulk ice temperature. In the case of first-year ice in the high Arctic, an attenuation factor of 2.4 was applied to the 10-day moving average of air temperature, after which an offset of 1.5 was applied to the measured air temperatures.

The figures show that the measured bulk ice temperature of first-year ice in the sub-Arctic is in good agreement with the estimated bulk ice temperature, part of the time. The best agreement between the measured and estimated bulk ice temperatures for Site S7 and Site A1 were from JD42 to JD55 (10 to 23 February, Figure 23-a) and from JD59 to JD71 (27 February to 11 March, Figure 23-b), respectively. After about JD95 (4 April) changes in the air temperature did not influence the bulk ice temperature of first-year ice in the sub-Arctic.

Figure 23-c compares the measured and estimated bulk ice temperature for first-year ice in the Arctic. Results show good agreement throughout most of the season, with the exception of the estimated bulk ice temperature being about 1.0°C lower than the measured value from JD142 to JD153 (22 May to 2 June). The comparison shows that the relation between the air temperature and the bulk ice temperature is more straightforward in the Arctic, than the sub-Arctic.

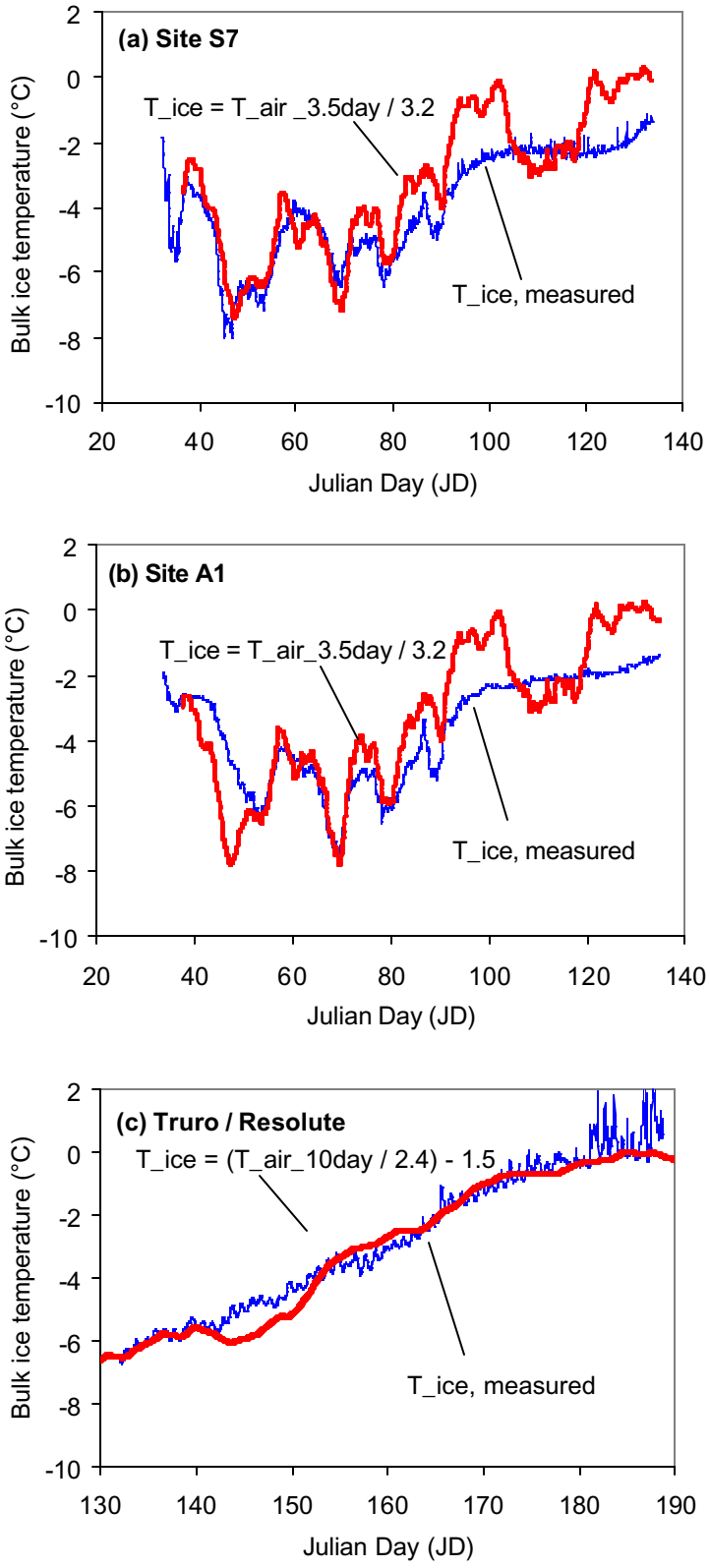

Figure 23 Estimating bulk ice temperature from air temperature data

8.0 Validating Output from CIS's Thermodynamic Model

The previous discussion showed that the technique of estimating the bulk ice temperature from the air temperature had promise, however it was not a straightforward process. In light of that, another option for obtaining the bulk temperature of the ice was explored: the thermodynamic model used by CIS. That thermodynamic model was developed by Flato and Brown (1996), and forecasts a number of parameters, including the air temperature, snow thickness, ice thickness and the temperature at ten equidistant layers throughout the full thickness of ice.

The accuracy of the forecasted data was determined by comparing output from the thermodynamic model to measurements made at each of the sampling sites in the high Arctic (in 2000, 2001, 2002) and the six sampling sites in the sub-Arctic (in 2004). Appendix B includes two tables comparing field measurements to (a) output from the thermodynamic model using cloud data as input and (b) output from the thermodynamic model using the CMC flux as input. The plots in this section include only data that were generated from the model using cloud data, since that model forcing is believed to be more accurate. Appendix B contains comparison plots for model using CMC flux.

8.1 Air Temperature

Figure 24 shows a comparison of the measured air temperature and the air temperatures forecasted by the thermodynamic model for each of the sampling sites in the (a) sub-Arctic[8] and (b) the high Arctic. In general, the model outputs air temperatures that are in reasonably good agreement with the measured air temperatures. Figure 24-c shows a cross-plot of the measured and modeled air temperatures. Most of the data points are above the line of 1:1 correspondence, which shows that the forecasted data are colder than the measured air temperatures.

8.2 Snow Thickness

Figure 25 shows a comparison of the measured and modeled snow thickness for (a) the sub-Arctic and (b) the high Arctic. Figure 25-a makes two points apparent: (i) there was considerable variability in the measured snow thicknesses at each of the six sites in Labrador and (ii) the actual snow thickness decreased as the season advanced, whereas the forecasted snow thickness continued to increase throughout the season. The cross-plot of the measured and forecasted snow thickness in Figure 25-c shows that, in general, the model over predicted snow thicknesses in the both sub-Arctic and the Arctic. There were occasions on which the model forecasted no snow cover when, in fact, the ice had a minimal layer of snow (those data points are plotted directly on the x-axis).

[8] Because the CIS model had a limited resolution, the forecasted data were the same for Sites S2, S6 and S10 in Strathcona Run (which were each separated by a distance of 4 km). Output from the model was the same at Sites A2, A6 and A10 in Anaktalak Run.

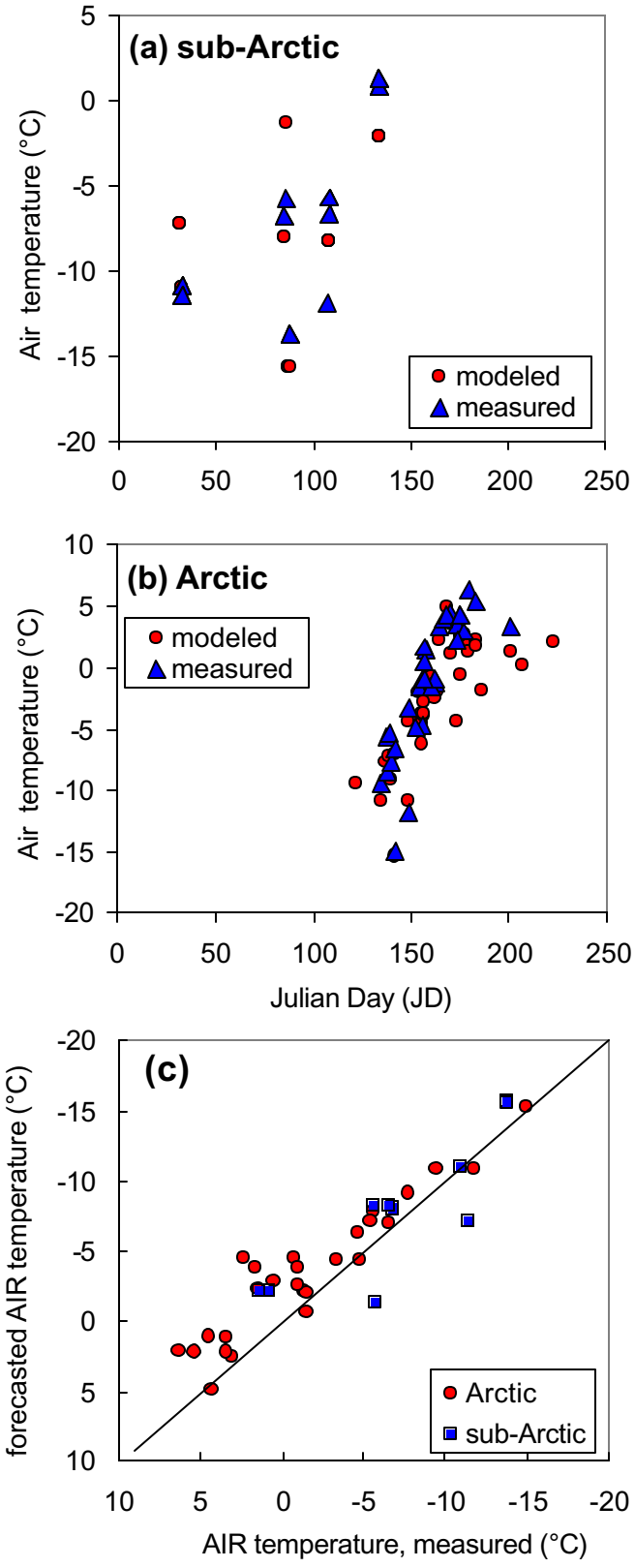

Figure 24 Air temperature: measured and modeled

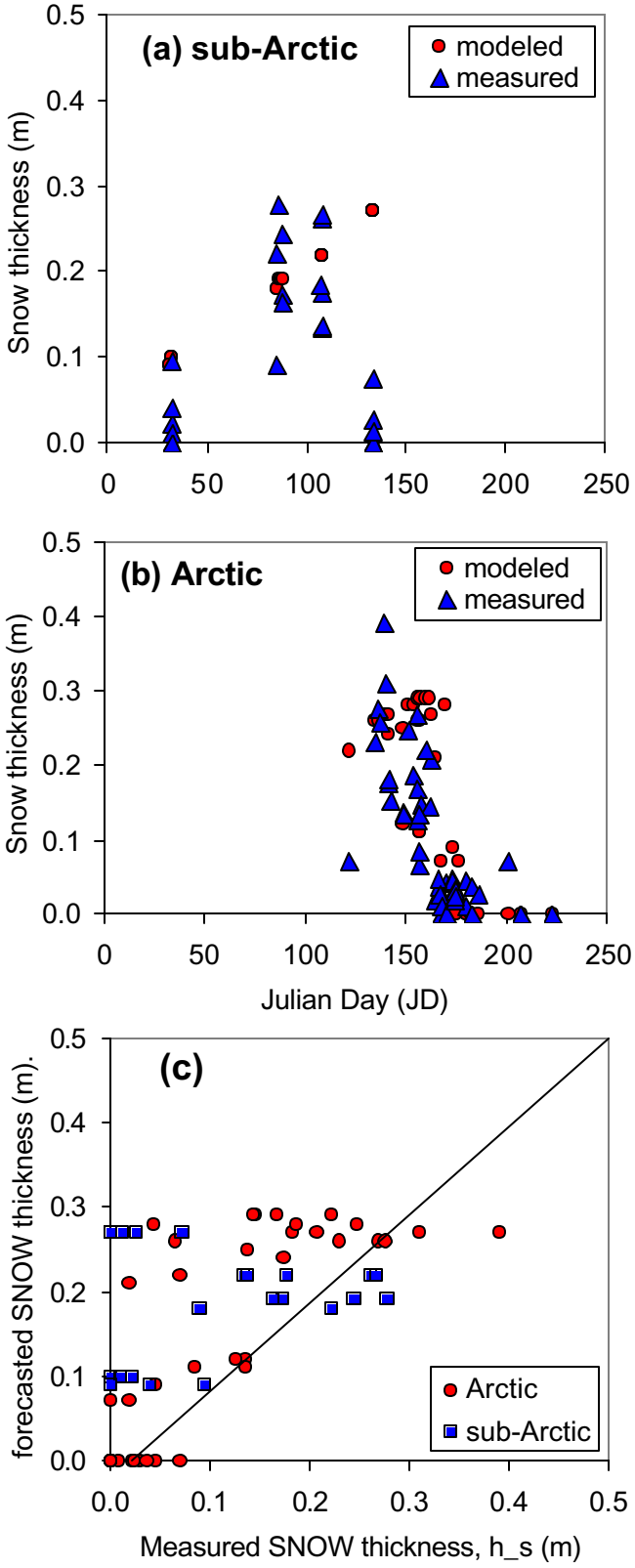

Figure 25 Snow thickness: measured vs. modeled

8.3 Ice Thickness

Figure 26 shows the measured and forecasted ice thickness for (a) sites in the sub-Arctic and (b) the high Arctic. Overall, there better good agreement between the measured and forecasted ice thicknesses of first-year ice in the sub-Arctic, than in the high Arctic. The model tended to overestimate ice thickness in the Arctic (Figure 26-c).

Three of the sampling sites in the high Arctic had considerable difference between the measured and modeled ice thickness. On 20 July 2000 (JD201), the measured ice thickness at Truro Island was 0.83 m, whereas the forecasted ice thickness was 1.13 m. On 26 July 2002 (JD207), the measured ice thickness in Allen Bay was 1.19 m, and the modeled ice thickness was 0.30 m. On 11 August 2002 (JD223), the ice thickness in the northern part of Allen Bay was 1.27 m, whereas the forecasted ice thickness was 0.0 m. Note that those three data points were in July or August.

8.4 Bulk Ice Temperature

Earlier, it was shown that errors in the bulk ice temperature have direct bearing on calculations of the flexural strength of the ice. Therefore, determining the accuracy with which the CIS model forecasts ice temperatures is, perhaps, more important than the determining how accurately it predicts the snow and ice thickness, or air temperatures (although it is acknowledged that those parameters may have direct bearing on the forecasted ice temperatures). The 10-layer thick, ice temperature profiles output by the CIS model were used to calculate the depth-averaged, bulk ice temperature.

Figure 27 shows a comparison of the measured and forecasted bulk ice temperatures for (a) the sub-Arctic and (b) the Arctic. The model consistently outputs bulk ice temperatures that are colder than the measured bulk ice temperatures in both the sub-Arctic and the Arctic. In general, there is lesser agreement between the measured and modeled bulk ice temperatures for first-year ice in the sub-Arctic, than the Arctic. As expected, the coldest bulk ice temperature occurred on 2 May (JD122) at the Barrow Site, the earliest date on which measurements were made in the high Arctic. The measured bulk ice temperature for the Barrow site was -8.99°C[9], and the forecasted bulk ice temperature was -9.92°C.

[9] The full ice thickness at the Barrow Site was not measured, and temperatures were measured in only the uppermost 1.5 m of ice. In all likelihood, the bulk ice temperature of the full thickness ice would have been slightly higher than -8.99°C.

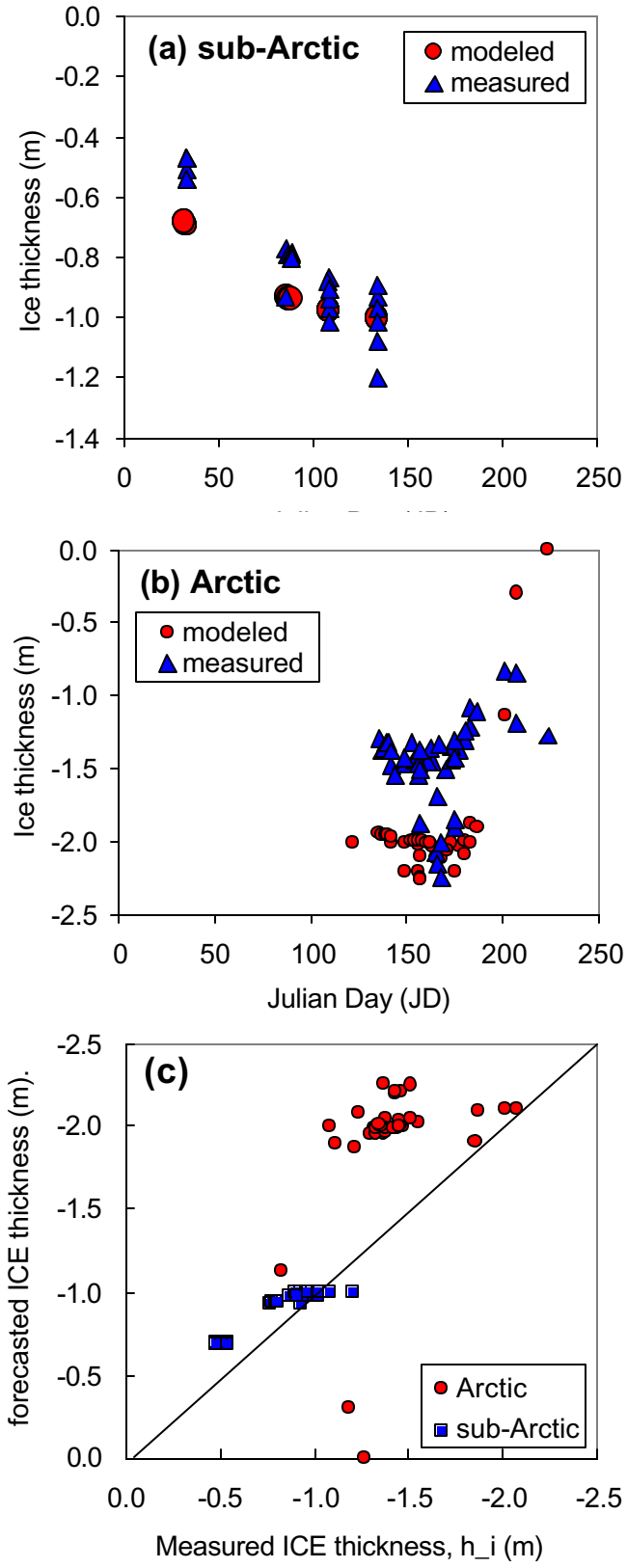

Figure 26 Ice thickness: measured vs. modeled

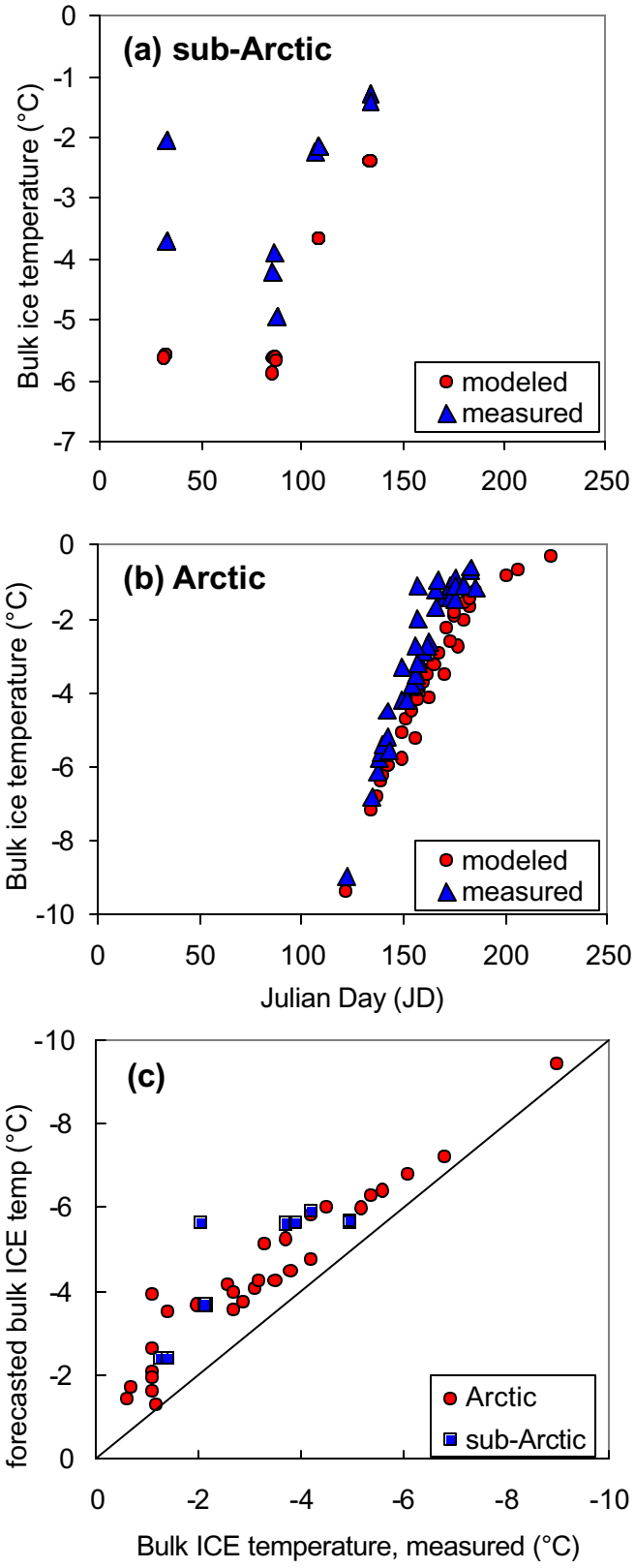

Figure 27 Bulk ice temperature: measured vs. modeled

9.0 Using Output from the CIS Model to Calculate the Flexural Strength

The previous discussion showed that the CIS model has greater promise for determining the bulk ice temperatures than the technique of using the moving average of air temperature. The bulk ice temperatures output by the model, which are reasonably accurate, may be used to calculate the flexural strength of the ice. This new approach will be called Approach D.

Figure 28 compares the flexural strengths from Approach D, where the bulk ice temperature and ice thickness were used in the calculation, to Approach A, which used the measured bulk salinity of the ice and the measured bulk ice temperature. Recall that Approach A is the more accurate means of calculating the flexural strength of the ice. Appendix C includes a table of values for the strengths calculated using Approach A and Approach D.

In general, the flexural strengths calculated from the modeling data (Approach D) were higher than those calculated from ice property measurements (Approach A). The data point that showed the least agreement (circled in Figure 28) corresponded to first-year ice at Griffith Island (74° 21.19' N, 94°56.10' W). When the ice was sampled on 6 June 2002 (JD157), its thickness was 1.37 m, the bulk ice temperature of the extracted core was -1.12°C, and the bulk ice salinity was 5.94‰. By comparison, the model forecasted an ice thickness of 2.26 m and a bulk ice temperature of -3.91°C. Because the first-year ice at Griffith Island had a relatively high salinity and was warm, its flexural strength should have been low on June 6.

In general, the reasonable agreement between results from Approach A and Approach D show that output from the CIS model can be used to calculate the strength of the ice when information about the ice properties is not available. although results will be conservative, in most cases.

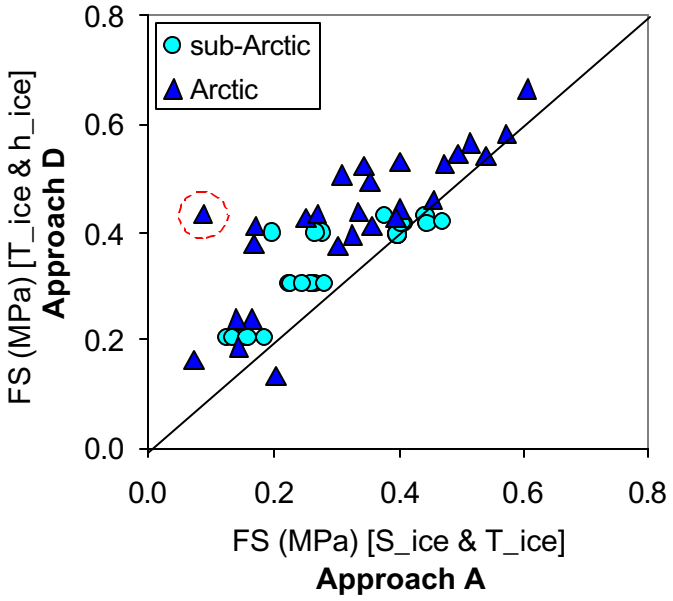

Figure 28 Using output from CIS model to calculate the flexural strength of the ice

9.1 Limit Dates for Calculating the Flexural Strength of the Ice

All of the discussed approaches for calculating the flexural strength of the ice are valid only within a specific range of ice temperatures, since they are based on an equation that describes the empirical relation between the measured flexural strength of the ice and the brine volume of the ice. Although Approach D may provide a viable method of calculating the flexural strength of the ice, without requiring information about the measured ice properties, it still suffers from the limitation that it can only be used until a certain date.

Figure 29 shows the approximate limit dates of Approach A and Approach D. The limit dates correspond to the approximate date on which the root brine volume fraction exceeds 0.5, the upper limit for Equation (1). In the sub-Arctic, Approach D can be used to calculate the flexural strength of the ice until mid-May (JD135), provided the technique of holding the salinity constant is used for the late-season measurements (as shown in Figure 19). In the Arctic, Approach D can be used to calculate the flexural strength of the ice until about early July (JD180). Note that Approach A, which requires having information about the ice properties, is also limited to the first week of July.

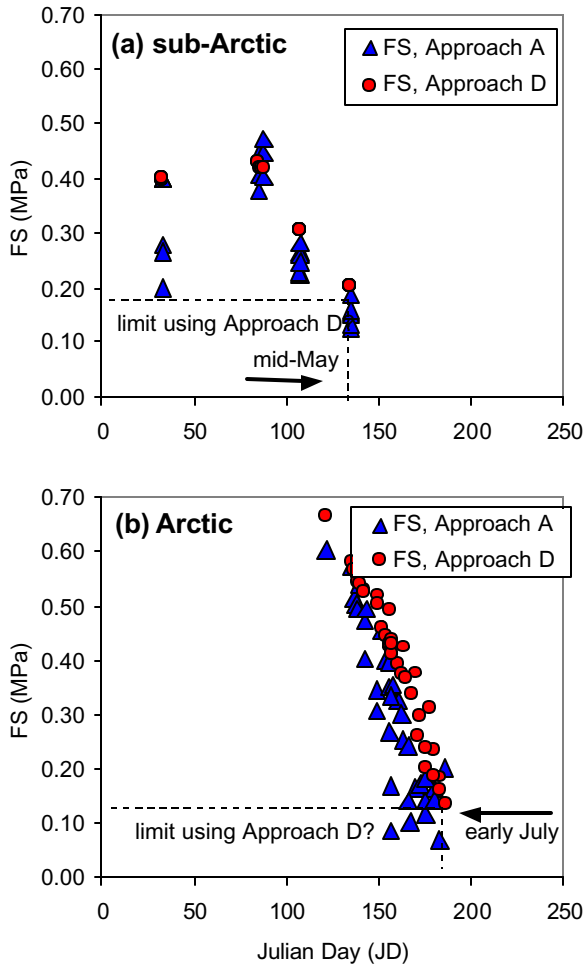

Figure 29 Limit dates for calculating the flexural strength using Approach D

10.0 Beyond the Calculated Flexural Strength: Borehole Strength

In order to determine whether it is necessary to calculate the flexural strength of the ice beyond the limit dates of Approach A and Approach D, it is useful to have information about how much further the ice strength decreases after mid-May (in the sub-Arctic) and early July (in the Arctic). Some other means must be used to determine the strength of the ice beyond the limit dates. Past field programs on decaying ice have shown that the borehole indentor can successfully measure the *in situ* strength of the ice until mid August, in the high Arctic. Although it would be possible to measure the borehole strength of first-year ice in the high Arctic after mid August, safely accessing the ice becomes a problem at that late date.

Figure 30 shows borehole strength data from the following

- tests conducted on young first-year ice in the Arctic during freeze-up in October 2003 (Johnston, 2004)
- data from existing literature on the borehole strength of Arctic first-year ice in winter (Blanchet et al., 1997; Sinha, 1986)
- three measurement seasons on decaying first-year ice in the Arctic (Johnston et al., 2001, 2002, 2003).
- recently conducted measurements on first-year ice in the sub-Arctic (Johnston, 2005).

There are several important points to note from the figure:

- the growth and decay season for first-year ice typically extends from September to late August in the Arctic, and from mid December to mid June in the sub-Arctic
- measurements show that Arctic first-year ice attains a maximum strength of about 30 MPa half-way through the season, in mid March (JD70)
- it can be inferred that first-year ice in the sub-Arctic also attains a maximum strength half-way through the season, in which case the ice would have a strength of about 17 or 18 MPa in mid March
- first-year ice in the Arctic and the sub-Arctic show similar trends of decreasing strength, however the strength of first-year ice in the sub-Arctic decreases about 60 days before the Arctic
- the strength of Arctic first-year ice reaches 10% of its mid-winter maximum (3 MPa) in early July (JD180), after which the ice strength remains stable at that level
- if first-year ice in the sub-Arctic is, in fact, 60 days ahead of the Arctic, the borehole strength should reach a strength plateau around JD120, in which case the strengths measured in Labrador in mid May (JD135) would be part of that plateau

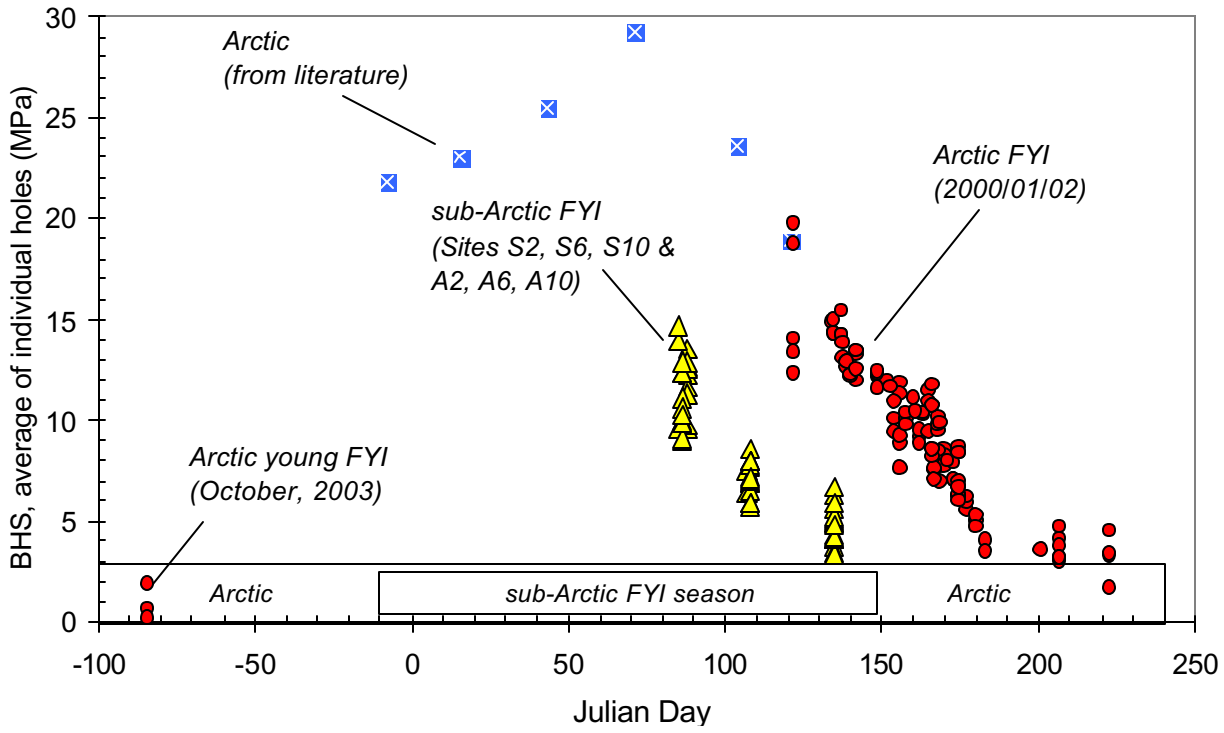

Figure 30 Seasonal increase and decrease in BHS for FYI in Arctic and sub-Arctic

Figure 29 showed that Approach D can be used to calculate the flexural strength of the ice until about mid May (JD135) in the sub-Arctic, and until early July (JD180) in the high Arctic. In mid May, the borehole strength of first-year ice in the sub-Arctic is about 5 MPa, or about 36% of its winter maximum strength of 17 to 18 MPa. Similarly, in early July, first-year ice in the high Arctic has a strength from 3 to 5 MPa, or roughly 10 to 15% of its mid winter maximum strength of 30 MPa).

Because field measurements have shown that the borehole strength and the calculated flexural strength of the ice decrease in a similar manner, it can be inferred that Approach D can be used to calculate the flexural strength until it is about 35% of its mid-winter strength in the sub-Arctic, and 10 to 15% of its winter maximum in the high Arctic. At present, it is not known whether the limits of Approach D can be extended into the region beyond those dates. Depending upon the intended objective of the Ice Strength Charts, it may not be necessary to calculate the flexural strength past the current limitations. If the strength is needed past mid May (sub-Arctic) or early July (Arctic), means must be explored to extend the calculation later in the season. That would likely require establishing a relation between the calculated flexural strength of the ice and the measured ice borehole strength. The relation is not a simple one however, as shown in the following section.

10.1 Relating Ice Borehole Strength to Calculated Flexural Strength

Figure 31 shows a comparison of the measured borehole strength and the flexural strength calculated using Approach A for (a) first-year ice in the sub-Arctic and (b) first-year ice in the high Arctic. It should be noted that, in May, the flexural strength of the sub-Arctic first-year ice was calculated using the salinity that was measured in April (using the technique of holding the salinity constant, as shown in Figure 19).

The correlation coefficient between the borehole strength (BHS) and flexural strength (FS) is 0.74 for first-year ice in the sub-Arctic and 0.70 for first-year ice in the Arctic. Clearly, the relation between the two strengths will need to be explored further, if the Ice Strength Charts are to include the calculated flexural strength after the previously discussed cut-off dates.

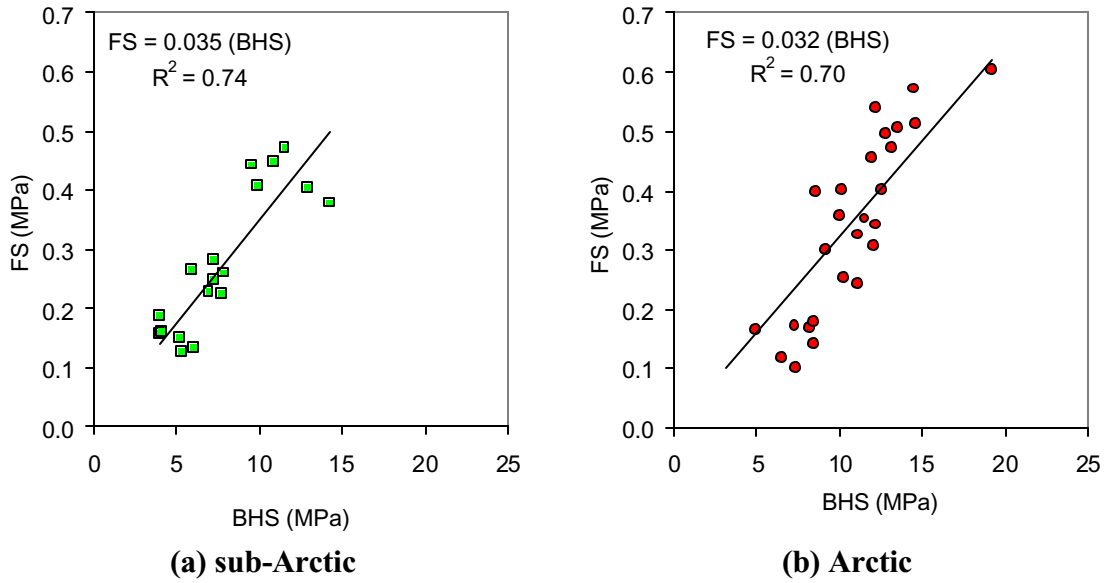

Figure 31 Measured borehole strength vs. calculated flexural strength
BHS: measured borehole strength; FS: calculated flexural strength

11.0 Conclusions

Realizing that one of CIS's objectives is to include both first-year ice in the high Arctic and the sub-Arctic in the Ice Strength Charts, it was suggested that future Charts express the seasonal decrease in ice strength in terms of the (calculated) flexural strength of the ice. The rationale for that approach stems from past strength tests in the high Arctic, which have shown that the *in situ* borehole strength of the ice and the calculated flexural strength of the ice decrease in a similar manner. In the past, the Ice Strength Charts used an empirical relation between the normalized ice strength (borehole strength and flexural strength) and the air temperature (using accumulated warming degree days). While that approach was effective for forecasting the strength of first-year ice in the high Arctic, it was not feasible for including first-year ice in the sub-Arctic in the Strength Charts.

This report presented various approaches for calculating the flexural strength of the ice, all of which required information about either the physical properties of the ice, the measured air temperatures and the ice thickness, or the modeled bulk ice temperature and ice thickness. Analysis showed that although an averaging technique can be applied to the air temperature record to reproduce changes in the bulk ice temperature, developing a relation between the air temperature and ice temperature is not straightforward. Part of the difficulty relates to the lack of information about the snow cover: little is known about changes in the snow thickness, metamorphosis of the snow cover, and changes in its thermal properties. All of those factors influence the rate at which air temperature fluctuations translate to the ice cover.

Having shown that relating changes in air temperature to the bulk ice temperature would require considerably more information than is currently available, output from the thermodynamic model that CIS uses, was explored as a means of determining the bulk temperature of the ice. The validity of the forecasted data (air temperatures, snow thickness, ice thickness and ice temperatures) was first assessed using measurements acquired during three seasons in the high Arctic, and one season in the sub-Arctic. The forecasted data and field measurements were in reasonably good agreement for both the sub-Arctic and high Arctic.

Preliminary analysis showed that output from the CIS thermodynamic model could be a viable means of calculating the flexural strength of the ice, albeit a conservative approach. Using model data as input, the flexural strength of first-year ice could be calculated until about mid May in the sub-Arctic, and until early July in the high Arctic. At that point, first-year ice in the sub-Arctic would have about 35% of its maximum winter strength. In early July, first-year ice in the high Arctic would have from 10 to 15% of its winter maximum strength. It should be noted that first-year ice in the sub-Arctic does not attain the strength of first-year ice in the high Arctic, as shown by the borehole strength data (maximum of 17 to 18 MPa in sub-Arctic and 30 MPa in high Arctic).

12.0 Recommendations

This report is concluded by asking, "what is the intended purpose of the Ice Strength Charts?" Realizing that the objective of the past two-years' work was to include sub-Arctic ice in the Ice Strength Charts, this report suggested an approach for doing so, using data from the CIS's thermodynamic model to calculate the flexural strength of the ice. Although preliminary analysis showed that approach to have potential, it is recommended that further work be conducted to validate output from the model using field measurements.

The second recommendation is that a meeting be held between all stakeholders (CIS, Transport Canada, Canadian Coast Guard, Industry). The objective of the meeting would be to determine how the Ice Strength Charts would best be utilized or adapted to suit the mariner, and to resolve the issue of whether the ice strength should be forecast beyond the cut-off dates suggested outlined in this report. Outcome from the meeting would guide further research in this area.

13.0 References

Blanchet, D., Abdelnour, R., and Comfort, G. (1997) Mechanical Properties of First-year Sea Ice at Tarsiut Island. J. Cold Regions Engineering, Vol. 1, pp. 59 - 83.

Dickins, D.F. and Dempsey, J.B. (2005) Ice Conditions used as a Design Basis for the Voisey's Bay Development. Proc. 18th Int. Conf. on Port and Ocean Eng. under Arctic Conditions (POAC'05), Potsdam, NY, USA, 26 - 30 June 2005, Vol. 1, pp. 131 -142.

Flato, G.M. and Brown, R.D. (1996) Variability and Climate Sensitivity of Landfast Arctic Sea Ice. J. Geophys. Res., 101 (C10), pp. 25,767-25,777.

Gauthier, M-F., DeAbreu, R., Timco, G.W. and Johnston, M.E. (2002) Ice Strength Information in The Canadian Arctic: From Science To Operations. Proc. of the 16th IAHR Int. Sym. on Ice, Dunedin, New Zealand, pp 203-210.

Johnston, M. (2004) Properties of Second-year and Multi-year Ice during Freeze-up. Technical Report CHC-TR-024. Submitted to Transport Canada, Ottawa, Ontario, Canada. March 2004. 26 p.

Johnston, M. (2005) Properties of Level Landfast Ice and Hummocked Ice near Nain, Labrador. Report CHC-TR-031, submitted to Transport Canada and Canadian Ice Service. Ottawa, Ontario. March 2005. 27 p.

Johnston, M. and Timco, G.W. (2002) Temperature Changes in First Year Arctic Sea Ice During the Decay Process. Proceedings of the 16th IAHR Int. Sym. on Ice, Dunedin, New Zealand, Vol., 2, pp. 194-202.

Johnston, M. and Timco, G. (2003) Developing an Ice Strength Algorithm for Level, Landfast First-year Ice in the High Arctic. Technical Report CHC-TR-13. Submitted to Canadian Ice Service. Ottawa, Ontario. March, 2003. 22 p.

Johnston, M. and Timco, G.W. (2004) Developing an Ice Strength Algorithm for Sub-Arctic Regions. Report CHC-TR-023. Submitted to Canadian Ice Service. March, 2004. 28 p.

Johnston, M., Frederking, R. and Timco, G. (2001) Decay-Induced Changes in the Physical and Mechanical Properties of First Year Ice. Proc. 16th Int. Conf. on Port and Ocean Eng. under Arctic Conditions, POAC'01, Ottawa, Canada, pp. 1395-1404.

Johnston, M., Frederking, R. and Timco, G. (2002) Properties of Decaying First Year Sea Ice: Two Seasons of Field of Field Measurements. Proc. 17th Int. Conf. on Okhotsk Sea and Sea Ice, Mombetsu, Hokkaido, Japan, pp. 303-311.

Johnston, M., Frederking, R. and Timco, G.W. (2003) Properties of Decaying First-year Sea Ice at Five Sites in Parry Channel. Proc. 17th Int. Conf. on Port and Ocean Eng. under Arctic Conditions, POAC'03, Trondheim, Norway, Vol. 1, pp. 131-140.

Langlois, D., DeAbreu, R., Gauthier, M.F., Timco, G.W. and Johnston, M. (2003): Early Results of the Canadian Ice Service Ice Strength Chart. Proc. 17th Int. Conf. on Port and Ocean Engineering under Arctic Conditions, Trondheim, Norway. Vol. 1, pp. 165 - 174.

Masterson, D. (1996): Interpretation of *In Situ* Borehole Ice Strength Measurement Tests. Can. J. Civ. Eng. Vol. 23. pp. 165- 179.

Timco, G. and Johnston, M. (2002) Sea Ice Strength during the Melt Season. IAHR, Proc. 16th Int. Sym. on Ice, Dunedin, New Zealand, 2 - 6 December 2002, pp. 187 - 193.

Timco, G. and O'Brien, S. (1994) Flexural Strength Equation for Sea Ice, J. Cold Regions Science and Technology, Vol. 22, pp. 285 - 298.

Sinha, N.K. (1986) "The Borehole Jack: Is it a Useful Tool?" Proc. of 5th Int. Offshore Mechanics and Arctic Engineering Symp. (OMAE). Tokyo, Japan. 13 – 17 April 1986. Vol. IV, pp. 328 – 335.

Appendix A: Sampling Methodology

Sampling Methodology

Different property measurements were made at different sites, as listed in Table 1. The sampling methodology required using a motor driven, fibreglass corer to make three boreholes in the ice (0.15 m diameter), each at least 2.0 m apart. The ice thickness, freeboard and snow depths were measured at each borehole. The cores removed from the three boreholes were used to measure either the temperature profile of the ice, or the salinity profile of the ice.

Ice Temperature

Ice temperatures were measured with a calibrated Fluke 73 multimeter, with an attached 80T-150U temperature probe. The temperature probe was inserted into small holes that had been made in the core at intervals of 200 mm (100 mm for the thinner ice in February). It should be noted that, when the temperature of the ice approaches its melting point, the accuracy of the probe decreases to ± 2°C.

The *in situ* temperature of the ice at Site S7 and Site A1 was measured by freezing temperature chains into the ice (Figure 8). Each temperature chain measured the temperature of the air, snow and ice at 30-minute intervals. A digital data logger recorded the measured temperatures from 1 February, when the chains were installed, until 14 May, when the chains were removed (Johnston and Timco, 2005). The temperature chain at Site S7 measured the temperature of the ice at depth intervals of 200 mm, to a depth of 1.4 m. The chain at Site A1 (which was initially intended for ridged ice) measured the ice temperature at 100 mm depth intervals to an ice depth of 0.30 m, and at 200 mm intervals below that depth.

Ice Salinity

The salinity of the ice was measured by cutting small pie-shaped discs, about 20 mm thick, from the core at 200 mm intervals (100 mm intervals in February). The sections were cut and bagged as quickly as possible to minimize brine drainage. After the bagged samples had melted, at room temperature, an Orion model 105A portable conductivity meter (accuracy 0.5%) was used to measure the salinity of the melt water.

The salinity of the underlying seawater was measured in each borehole using a small bottle, with an attached rod. The borehole was first cleared of any ice left floating in the hole. The small bottle was then plunged about 0.50 m below the water, to minimize the amount of ice debris that was collected from each hole. The salinity of the seawater was measured after the sample had reached room temperature.

Borehole Strength

Once a borehole had been made in the ice, and its core had been processed, the ice strength in the borehole was measured at depth intervals of 0.30 m, until the bottom of the ice was reached. The NRCC borehole indentor was used to measure the *in situ* confined compressive strength of the ice. The NRCC borehole indentor consists of a high-strength stainless steel hydraulic cylinder with a laterally acting piston and two indentor plates, both of which are curved to match the wall of the borehole (Sinha, 2005). A 10,000 psi electro-hydraulic pump, with an average flow rate of 20 in^3/min, was used to activate the two pistons inside the body of the indentor and extend both indentor plates.

Throughout the tests, an external digital data acquisition system was used to record the displacement of each indentor plate and the oil pressure. While the pressure during a test was monitored using a dial gauge, a handheld keypad was used to provide output the indentor displacement. That ensured that the 10,000 psi capacity of the system and the 50 mm total diametrical displacement of the indentor plates were approached, but not exceeded. The indentor plates were fully retracted after each test, the borehole indentor was rotated 90° and the test unit was lowered to the next depth.

The ice borehole strengths in this report used a conversion factor of 0.56 to convert the measured oil pressure to an ice pressure. The conversion factor was determined from the ratio of the area on which the hydraulic fluid acts (3768 mm^2) to the surface area of the indentor plate (6692 mm^2). All ice borehole strengths are given for an indentor penetration of 3 mm (Johnston et al., 2001) and are compensated for the stress-rate effect using the procedure outlined in Johnston et al. (2003). Studies have shown that the ice borehole strength is almost twice that of the confined compressive strength of the ice measured in the laboratory (Sinha, 1986) and three to four times greater than the ice strength measured in unconfined tests (Masterson, 1996; Sinha, 1986).

References

Johnston, M., Frederking, R. and Timco, G. (2001) Decay-Induced Changes in the Physical and Mechanical Properties of First Year Ice. Proc. 16th Int. Conf. on Port and Ocean Eng. under Arctic Conditions, POAC'01, Ottawa, Canada, pp 1395-1404.

Johnston, M., Frederking, R. and Timco, G.W. (2003) Properties of Decaying First-year Sea Ice at Five Sites in Parry Channel. Proc. 17th Int. Conf. on Port and Ocean Eng. under Arctic Conditions, POAC'03, Trondheim, Norway, Vol. 1, pp 131-140.

Masterson, D. (1996): Interpretation of *In Situ* Borehole Ice Strength Measurement Tests. Can. J. Civ. Eng. Vol. 23. pp. 165- 179.

Sinha, N.K. (1986) "The Borehole Jack: Is it a Useful Tool?" Proc. of 5th Int. Offshore Mechanics and Arctic Engineering Symp. OMAE'86. Tokyo, Japan. 13 – 17 April 1986. Vol. IV. pp. 328 – 335.

Sinha, N.K. (2005): NRCC Borehole Indentor: Measuring Ice Strength. Proc. of 18th Int. Conf. on Port and Ocean Eng. under Arctic Conditions, POAC'05. Potsdam, New York, U.S.A. 20 - 26 June 2005, Vol. 1, pp. 153 - 164.

Appendix B: Field Measurements vs. Forecasted Data from CIS Model

Table B-1 Field Measurements vs. Forecasted Data (using cloud cover)

Field measurements in the sub-Arctic								CIS forecasted data for the sub-Arctic						
YEAR	JD	Site	T_air (°C)	h_s (m)	h_i (m)	Bulk ice temp (°C)	Bulk Salinity (‰)	JD	Site	T_air (°C)	h_s (m)	h_i (m)	Bulk ice temp (°C)	Lat/Long
2004	33	S2	-10.90	0.02	-0.54	-3.70	4.60	33	S2	-10.98	0.10	-0.69	-5.58	6269484N, 0582488W
2004	33	S6	-10.90	0.00	-0.47	-3.70	4.6	33	S4	-10.98	0.10	-0.69	-5.58	6269626N, 0584471W
2004	33	S10	-10.90	0.01	-0.51	-3.70	4.6	33	S10	-10.98	0.10	-0.69	-5.58	6269626N, 0584471W
2004	85	S2	-6.75	0.09	-0.93	-4.20	5.60	85	S2	-8.01	0.18	-0.93	-5.90	6269484N, 0582488W
2004	85	S6	-6.75	0.22	-0.77	-4.20	4.50	85	S4	-8.01	0.18	-0.93	-5.90	6269626N, 0584471W
2004	86	S10	-5.73	0.28	-0.79	-3.89	4.7	85	S10	-1.3	0.19	-0.94	-5.63	6269736N, 0590452W
2004	108	S2	-5.62	0.26	-0.97	-2.14	4.40	108	S2	-8.25	0.22	-0.98	-3.67	6269484N, 0582488W
2004	108	S6	-5.62	0.18	-0.87	-2.14	5.20	108	S4	-8.25	0.22	-0.98	-3.67	6269626N, 0584471W
2004	108	S10	-5.62	0.13	-0.94	-2.14	4.50	108	S10	-8.25	0.22	-0.98	-3.67	6269626N, 0584471W
2004	134	S2	+0.85	0.00	-0.93	-1.29	2.30	134	S2	-2.07	0.27	-1.00	-2.40	6269484N, 0582488W
2004	134	S6	+0.85	0.03	-0.97	-1.29	2.90	134	S4	-2.07	0.27	-1.00	-2.40	6269626N, 0584471W
2004	134	S10	+0.85	0.00	-0.89	-1.29	2.50	134	S10	-2.07	0.27	-1.00	-2.40	6269626N, 0584471W
2004	33	A2	-11.46	0.10	-0.47	-2.05	4	32	A2	-7.16	0.15	-0.57	-4.94	6253375N, 0584030W
2004	33	A6	-11.46	0.04	-0.47	-2.05	4.20	32	A4	-7.16	0.15	-0.57	-4.93	6253203N, 0586031W
2004	33	A10	-11.46	0.00	-0.54	-2.05	5.6	32	A10	-7.16	0.15	-0.57	-4.92	6253865N, 0591905W
2004	88	A2	-13.72	0.17	-0.78	-4.96	5.20	87	A2	-15.65	0.25	-0.80	-5.46	6253375N, 0584030W
2004	88	A6	-13.72	0.16	-0.79	-4.96	6.00	87	A4	-15.65	0.25	-0.80	-5.44	6253203N, 0586031W
2004	88	A10	-13.72	0.24	-0.80	-4.96	4.80	88	A10	-15.59	0.25	-0.80	-5.45	6253865N, 0591905W
2004	107	A2	-11.89	0.19	-0.88	-2.24	5.40							
2004	108	A6	-6.57	0.14	-0.90	-2.12	4.70	108	A4	-8.25	0.22	-0.98	-3.67	6253203N, 0586031W
2004	108	A10	-6.57	0.27	-1.02	-2.12	4.10	108	A10	-8.25	0.22	-0.98	-3.67	6253865N, 0591905W
2004	134	A2	+1.31	0.07	-1.08	-1.41	3.20	134	A2	-2.07	0.27	-1.00	-2.4	6253375N, 0584030W
2004	134	A6	+1.31	0.00	-1.02	-1.41	3.50	134	A4	-2.07	0.27	-1.00	-2.4	6253203N, 0586031W
2004	134	A10	+1.31	0.01	-1.20	-1.41	2.00	134	A10	-2.07	0.27	-1.00	-2.4	6253865N, 0591905W

NOTES:

- The measured mean daily air temperatures and bulk ice temperatures for sites in Strathcona Run were obtained from the temperature chain at Site S7. Similarly, the air temperature and bulk ice temperature for sites in Anaktalak Run were obtained from the temperature chain at Site A1.
- The snow and ice thickness are the average measurements from (up to) three boreholes at each site.
- The measured bulk ice salinity was obtained by depth-averaging measurements made on the extracted ice cores.
- Due to the resolution of the CIS thermodynamic model, forecasted data were not available for individual sites -- only for the general area in Strathcona Run and Anaktalak Run (forecasted data at Sites S2, S4 and S10 were the same, as were data for Sites A2, A4 and A10 -- for the same Julian Day).

Field measurements in the high Arctic								CIS forecasted data for the high Arctic						
YEAR	JD	Site	T_air (°C)	h_s (m)	h_i (m)	Bulk ice temp (°C)	Bulk Salinity (‰)	JD	Site	T_air (°C)	h_s (m)	h_i (m)	Bulk ice temp (°C)	Lat/Long
2000	142	Truro	-14.9	0.18	-1.47	-4.5	5.5	142	Truro	-15.3	0.24	-2.00	-6	75°13.94'N, 97°00.24'W
2000	149	Truro	-11.8	0.14	-1.46	-4.2	6.3	149	Truro	-10.82	0.25	-2.01	-5.8	75°13.94'N, 97°00.24'W
2000	156	Truro	-4.7	0.27	-1.55	-3.7	5.4	156	Truro	-6.24	0.26	-2.02	-5.23	75°13.94'N, 97°00.24'W
2000	163	Truro	-1.3	0.21	-1.45	-2.6	5.6	163	Truro	-2.04	0.27	-2.03	-4.15	75°13.94'N, 97°00.24'W
2000	170	Truro	4.5	0.04	-1.51	-1.4	4.5	170	Truro	1.1	0.28	-2.04	-3.5	75°13.94'N, 97°00.24'W
2000	173	Truro	3.5	0.05	-1.43	-1.4	4.4	173						
2000	177	Truro	3	0.02	-1.38		4	177	Truro	2.61	0.07	-2.04	-2.75	75°13.94'N, 97°00.24'W
2000	180	Truro	6.3	0.01	-1.31	-1.1	3.6	180	Truro	2.06	0.00	-1.99	-2.07	75°13.94'N, 97°00.24'W
2000	183	Truro	5.3	0.00	-1.21	-0.7		183	Truro	2.26	0.00	-1.88	-1.7	75°13.94'N, 97°00.24'W
2000	201	Truro	3.4	0.07	-0.83		0.5	201	Truro	1.26	0.00	-1.13	-0.86	75°13.94'N, 97°00.24'W
2001	135	Truro	-9.4	0.23	-1.30	-6.8	4.7	135	Truro	-10.81	0.26	-1.95	-7.21	75°13.94'N, 97°00.24'W
2001	137	Truro	-5.6	0.28	-1.37	-6.1	5.1	137	Truro	-7.81	0.26	-1.96	-6.81	75°13.94'N, 97°00.24'W
2001	138	Truro	-8.4	0.26	-1.36	-5.8	5	138						
2001	139	Truro	-5.4	0.39	-1.33	-5.6	5	139	Truro	-7.13	0.27	-1.96	-6.38	75°13.94'N, 97°00.24'W
2001	140	Truro	-7.7	0.31	-1.33	-5.4	4.2	140	Truro	-9.13	0.27	-1.96	-6.27	75°13.94'N, 97°00.24'W
2001	142	Truro	-6.6	0.18	-1.38	-5.2	5	142	Truro	-7.01	0.27	-1.97	-5.97	75°13.94'N, 97°00.24'W
2001	152	Truro	-4.8	0.25	-1.32	-4.2	4.3	152	Truro	-4.35	0.28	-1.99	-4.74	75°13.94'N, 97°00.24'W
2001	154	Truro	-1.5	0.19	-1.44	-3.8	4.7	154	Truro	-1.97	0.28	-1.99	-4.48	75°13.94'N, 97°00.24'W
2001	156	Truro	-0.8	0.17	-1.38	-3.5	4.4	156	Truro	-4.49	0.29	-1.99	-4.22	75°13.94'N, 97°00.24'W
2001	158	Truro	1.4	0.15	-1.41	-3.1	4.5	158	Truro	-2.22	0.29	-1.99	-4.02	75°13.94'N, 97°00.24'W
2001	160	Truro	-1.5	0.22	-1.45	-2.9	4.7	160	Truro	-0.66	0.29	-2.00	-3.75	75°13.94'N, 97°00.24'W
2001	162	Truro	-1.0	0.15	-1.35	-2.7	4.8	162	Truro	-2.58	0.29	-2.00	-3.52	75°13.94'N, 97°00.24'W
2001	173	Truro	2.3	0.05	-1.34	-1.1		173	Truro	-4.42	0.09	-2.01	-2.62	75°13.94'N, 97°00.24'W
2002	122	122_Bar		0.07		-8.99	5.50	122	Barrow (B1)	-9.45	0.22	-2.01	-9.37	74°51'10.5" N, 97°07'41.4"' W
2002	143	143_Truro		0.15	-1.55	-5.58	4.98							
2002	149	149_Truro	-3.3	0.14	-1.43	-3.31	5.70	149	Truro	-4.3	0.12	-2.20	-5.11	74°54.69' N, 97° 13.33' W
2002	156	156_Truro		0.13	-1.46	-2.70	5.46	156	Truro	-3.84	0.12	-2.21	-3.97	74°54.69' N, 97° 13.33' W
2002	157	157_Bar	-1	0.07	-1.87	-3.21	5.00	157	Barrow (B3)	-3.88	0.26	-2.10	-4.22	74° 50.72' N, 97°07.50' W
2002	157	157_Leo	0.5	0.14	-1.51	-1.99	6.28	157	Leopold (L2)	-2.83	0.11	-2.25	-3.65	74° 18.26' N, 91° 05.46' W
2002	157	157_Grif	1.7	0.09	-1.37	-1.12	5.94	157	Griffith (G2)	-3.78	0.11	-2.26	-3.91	74° 21.19' N, 94°56.10' W
2002	165	165_AB(I)	3.4	0.02	-2.07		4.06	165	AB(1)	2.23	0.21	-2.11	-3.28	74°43.97' N, 95°15.00' W
2002	166	166_Bar	4	0.04	-2.15	-1.70	3.87							

2002	166	166_Leo		0.05	-1.69	-1.23	4.56							
2002	167	167_Grif		0.03	-1.33	-0.95	4.49							
2002	168	168_AB(I)	4.3	0.00	-2.01			168	AB(1)	4.98	0.07	-2.11	-2.95	74°43.97' N, 95°15.00' W
2002	168	168_AB(M)		0.01	-2.24		3.87							
2002	171	171_AB(I)		0.00				171	AB(1)	3.53	0.00	-2.06	-2.24	74°43.97' N, 95°15.00' W
2002	175	175_Bar	4.3	0.02	-1.90	-1.47	4.41							
2002	175	175_Grif	4.3	0.03	-1.30	-0.88	3.74							
2002	175	175_Truro		0.03	-1.43	-1.11	4.10	175	Truro	-0.56	0.00	-2.21	-1.93	74°54.69' N, 97° 13.33' W
2002	175	175_AB(I)		0.02	-1.86		3.25	175	AB(1)	2.49	0.00	-1.91	-1.82	74°43.97' N, 95°15.00' W
2002	180	180_Truro		0.05	-1.24	-1.11	4.06	180	Truro	1.28	0.00	-2.09	-1.6	74°54.69' N, 97° 13.33' W
2002	183	183_Truro		0.04	-1.08	-0.60	3.60	183	Truro	1.82	0.00	-2.00	-1.44	74°54.69' N, 97° 13.33' W
2002	186	186_Truro		0.03	-1.11	-1.18	3.20	186	Truro	-1.79	0.00	-1.90	-1.28	74°54.69' N, 97° 13.33' W
2002	207	207_AB1(I)		0.00	-1.19		0.13	207	AB(2)	0.19	0.00	-0.30	-0.68	74°43.23' N, 95°04.46' W
2002	207	207_AB2(I)		0.00	-0.85		0.03							
2002	223	223_CAB		0.00	-1.27		0.46	223	AB(3)	2.18	0.00	0.00	-0.35	74°46.15' N, 95°17.29' W

CORRESPONDANCE ABOUT FORECASTED DATA

Michelle,

I've attached a new version of the CIS modeling comparison spreadsheet. I apologize for the problems with the previous one.

In our previous conversations, I mentioned that for our operational model we use CMC fluxes directly. We are now moving away from that to using cloud data, because we've discovered that the model doesn't perform well when forced with flux data directly. I've therefore used cloud data to generate this new spreadsheet.

Other parameters used were:
Mixing layer depth: 21 m
Time steps per day: 3
Snowfall: 0.0011 mm/day for Arctic sites, 0.0017 mm/day for Labrador sites

I've also realized that I was mistaken about the layer thicknesses changing; at the time the temperature profile was printed, they were evenly spaced.

I hope that's everything you need. Tom or I will send you my report either today or Monday. I'll be here until late today if you need any more information.

-- Troy

<<CIS_modeling_comparison.fixed.xls>>

-----Original Message-----
From: Moure,Troy [CIS] [mailto:Troy.Moure@ec.gc.ca]
Sent: Monday, August 23, 2004 11:09 AM
To: Johnston, Michelle
Subject: RE: Ice thickness model

Michelle,

In answer to your question, the temperatures are not necessarily equally spaced since the layers change thickness individually during each time step. However, they should be roughly equally spaced, since the thicknesses
are reset at the end of each time step.

Also, I wanted to let you know about a problem with the data I sent. The model can either be given downward longwave and shortwave heat fluxes directly, or it can be given a cloud amount (%) from which it computes the
fluxes itself.

For your data, I had intended to feed the model the fluxes directly, since that's what we do for our operational version. However, the model was attempting to use cloud amount instead (which was entirely my fault).

Since I wasn't giving it that data, it was using a cloud amount of 0 for the entire run.

I did test the model at Resolute (when it still had the same problem) and it worked fairly well, so it shouldn't be a huge problem. Still, I'll regenerate your data using the fluxes properly and send it to you. I'll also put in the layer
thicknesses along with the temperature profile.

Also, Tom recently contacted CMC about getting snowfall data for our grid. I'm using a fixed rate of 1.7 mm/day to generate your data; the accuracy should improve if the model is modified to use per-point snowfall data instead. If
we do get CMC snowfall data, it's something to consider for the future.

Finally, my last day is this Friday (the 27th). I'm working on a report discussing the behaviour of the model which I can send to you later this week, if you'd like.

-- Troy
-----Original Message-----
From: Johnston, Michelle [mailto:Michelle.Johnston@nrc-cnrc.gc.ca]
Sent: August 23, 2004 10:26 AM
To: Moure,Troy [CIS]
Subject: RE: Ice thickness model

Troy,

Thank you for the model output. I only examined it in passing, but it looks like just what we needed. One question: your ice temperatures are given at 10 equally spaced depths, that depend upon the ice thickness? For instance, 1.7 m thick ice results in 17 cm intervals and 2.0 m thick ice results in 20 cm intervals?

I may have more questions for you, as I get into the comparison.

Thank you.
Michelle
M. Johnston, PhD
Canadian Hydraulics Centre
National Research Council
Bldg. M-32, Montreal Road
Ottawa, Ontario K1A 0R6
phone: 613.990.5141 fax: 613.952.7679

-----Original Message-----
From: Moure,Troy [CIS] [mailto:Troy.Moure@ec.gc.ca]
Sent: Friday, August 13, 2004 2:26 PM
To: Johnston, Michelle
Cc: Carrieres,Tom [CIS]
Subject: RE: Ice thickness model

Hello Michelle,

Here's the CIS modeling comparison spreadsheet you asked for. Sorry for the delay. Here are a few details on how I generated the data:

I extracted atmospheric forcing data from the CMC data we use for our other models. I used the global grid, which has points spaced 1 lat/lon degree apart. There is no precipitation data available for this grid, so I used annual snowfall rates from Resolute station for the Arctic sites. For the Labrador sites I used a fixed snowfall rate of 1.7 mm/day, which is what Greg Flato used as a default rate in his code.

I set the mixing layer depth to 25m and ran the model for three time steps per day.

I omitted several Labrador sites because they were so close together that the model wouldn't have been able to capture the differences between them, given the granularity of the meteorological data.

I hope this helps. If you need anything else, feel free to contact me.

-- Troy

<<CIS_modeling_comparison.xls>>

Table B-2 Field Measurements vs. Forecasted data (using CMC input)

Field measurements in the sub-Arctic								CIS forecasted data for the sub-Arctic						
YEAR	JD	Site	T_air (°C)	h_s (m)	h_i (m)	Bulk ice temp (°C)	Bulk Salinity (‰)	JD	Site	T_air (°C)	h_s (m)	h_i (m)	Bulk ice temp (°C)	Lat/Long
2004	33	S2	-10.90	0.02	-0.54	-3.70	4.60	33	S2	-9.86	0.15	-0.57	-4.9	6269484N, 0582488W
2004	33	S6	-10.90	0.00	-0.47	-3.70	4.6	33	S4	-9.84	0.15	-0.57	-4.9	6269626N, 0584471W
2004	33	S10	-10.90	0.01	-0.51	-3.70	4.6	33	S10	-9.84	0.15	-0.57	-4.9	6269626N, 0584471W
2004	85	S2	-6.75	0.09	-0.93	-4.20	5.60	85	S2	-11.63	0.24	-0.79	-5.78	6269484N, 0582488W
2004	85	S6	-6.75	0.22	-0.77	-4.20	4.50	85	S4	-11.64	0.24	-0.79	-5.78	6269626N, 0584471W
2004	86	S10	-5.73	0.28	-0.79	-3.89	4.7	85	S10	-11.67	0.24	-0.79	-5.78	6269736N, 0590452W
2004	108	S2	-5.62	0.26	-0.97	-2.14	4.40	108	S2	-15.37	0.28	-0.84	-3.75	6269484N, 0582488W
2004	108	S6	-5.62	0.18	-0.87	-2.14	5.20	108	S4	-15.37	0.28	-0.84	-3.75	6269626N, 0584471W
2004	108	S10	-5.62	0.13	-0.94	-2.14	4.50	108	S10	-15.37	0.28	-0.84	-3.75	6269736N, 0590452W
2004	134	S2	+0.85	0.00	-0.93	-1.29	2.30	134	S2	-1.03	0.30	-0.87	-2.26	6269484N, 0582488W
2004	134	S6	+0.85	0.03	-0.97	-1.29	2.90	134	S4	-1.03	0.30	-0.87	-2.26	6269626N, 0584471W
2004	134	S10	+0.85	0.00	-0.89	-1.29	2.50	134	S10	-1.03	0.30	-0.87	-2.26	6269736N, 0590452W
2004	33	A2	-11.46	0.10	-0.47	-2.05	4	32	A2	-5.9	0.15	-0.57	-4.94	6253375N, 0584030W
2004	33	A6	-11.46	0.04	-0.47	-2.05	4.20	32	A4	-5.87	0.15	-0.57	-4.93	6253203N, 0586031W
2004	33	A10	-11.46	0.00	-0.54	-2.05	5.6	32	A10	-5.81	0.15	-0.57	-4.92	6253865N, 0591905W
2004	88	A2	-13.72	0.17	-0.78	-4.96	5.20	87	A2	-15.67	0.25	-0.80	-5.46	6253375N, 0584030W
2004	88	A6	-13.72	0.16	-0.79	-4.96	6.00	87	A4	-15.64	0.25	-0.80	-5.44	6253203N, 0586031W
2004	88	A10	-13.72	0.24	-0.80	-4.96	4.80	88	A10	-16.45	0.25	-0.80	-5.45	6253865N, 0591905W
2004	107	A2	-11.89	0.19	-0.88	-2.24	5.40	108	A2	-14.82	0.28	-0.84	-3.65	6253375N, 0584030W
2004	108	A6	-6.57	0.14	-0.90	-2.12	4.70	108	A4	-14.82	0.28	-0.84	-3.65	6253203N, 0586031W
2004	108	A10	-6.57	0.27	-1.02	-2.12	4.10	108	A10	-14.82	0.28	-0.84	-3.65	6253865N, 0591905W
2004	134	A2	+1.31	0.07	-1.08	-1.41	3.20	134	A2	-1.06	0.30	-0.87	-2.2	6253375N, 0584030W
2004	134	A6	+1.31	0.00	-1.02	-1.41	3.50	134	S4	-1.06	0.30	-0.87	-2.2	6253203N, 0586031W
2004	134	A10	+1.31	0.01	-1.20	-1.41	2.00	134	A10	-1.06	0.30	-0.87	-2.2	6253865N, 0591905W

NOTES:

- The measured mean daily air temperatures and bulk ice temperatures for sites in Strathcona Run were obtained from the temperature chain at Site S7. Similarly the air temperature and bulk ice temperature for sites in Anaktalak Run were obtained from the temperature chain at Site A1.
- The snow and ice thickness are the average measurements from (up to) three boreholes at each site.
- The measured bulk ice salinity was obtained by depth-averaging measurements made on the extracted ice cores.
- Depending upon the site, the Julian Day on which some sites were sampled differed from the dates for which the CIS forecasted data were supplied, by up to a day.
- Due to the resolution of the CIS thermodynamic model, forecasted data were not available for individual sites -- only for the general area in Strathcona Run and Anaktalak Run (forecasted data at Sites S2, S4 and S10 were the same, as were data for Sites A2, A4 and A10 -- for the same Julian Day).
- Note there are variations from 0.01 to 0.04°C in the air temperatures forecasted at the different sites in Strathcona Run and Anaktalak Run.

Field measurements in the high Arctic								CIS forecasted data for the high Arctic						
YEAR	JD	Site	T_air (°C)	h_s (m)	h_i (m)	Bulk ice temp (°C)	Bulk Salinity (‰)	JD	Site	T_air (°C)	h_s (m)	h_i (m)	Bulk ice temp (°C)	Lat/Long
2000	142	Truro	-14.9	0.18	-1.47	-4.5	5.5	142	Truro	-12.77	0.34	-1.80	-5.14	75°13.94'N, 97°00.24'W
2000	149	Truro	-11.8	0.14	-1.46	-4.2	6.3	149	Truro	-10.42	0.35	-1.81	-4.92	75°13.94'N, 97°00.24'W
2000	156	Truro	-4.7	0.27	-1.55	-3.7	5.4	156	Truro	-6.27	0.36	-1.82	-4.52	75°13.94'N, 97°00.24'W
2000	163	Truro	-1.3	0.21	-1.45	-2.6	5.6	163	Truro	1.11	0.37	-1.82	-3.45	75°13.94'N, 97°00.24'W
2000	170	Truro	4.5	0.04	-1.51	-1.4	4.5	170	Truro	2.71	0.35	-1.83	-3	75°13.94'N, 97°00.24'W
2000	173	Truro	3.5	0.05	-1.43	-1.4	4.4	173						
2000	177	Truro	3	0.02	-1.38		4	177	Truro	2.95	0.00	-1.76	-1.86	75°13.94'N, 97°00.24'W
2000	180	Truro	6.3	0.01	-1.31	-1.1	3.6	180	Truro	2.91	0.00	-1.57	-1.44	75°13.94'N, 97°00.24'W
2000	183	Truro	5.3	0.00	-1.21	-0.7		183	Truro	2.6	0.00	-1.35	-1.16	75°13.94'N, 97°00.24'W
2000	201	Truro	3.4	0.07	-0.83		0.5	201	Truro	1.9	0.00		-0.95	75°13.94'N, 97°00.24'W
2001	135	Truro	-9.4	0.23	-1.30	-6.8	4.7	135	Truro	-10.78	0.28	-1.96	-6.8	75°13.94'N, 97°00.24'W
2001	137	Truro	-5.6	0.28	-1.37	-6.1	5.1	137	Truro	-7.05	0.29	-1.96	-6.39	75°13.94'N, 97°00.24'W
2001	138	Truro	-8.4	0.26	-1.36	-5.8	5	138						
2001	139	Truro	-5.4	0.39	-1.33	-5.6	5	139	Truro	-5.74	0.29	-1.97	-5.97	75°13.94'N, 97°00.24'W
2001	140	Truro	-7.7	0.31	-1.33	-5.4	4.2	140	Truro	-8.44	0.29	-1.97	-5.87	75°13.94'N, 97°00.24'W
2001	142	Truro	-6.6	0.18	-1.38	-5.2	5	142	Truro	-6.23	0.29	-1.97	-5.55	75°13.94'N, 97°00.24'W
2001	152	Truro	-4.8	0.25	-1.32	-4.2	4.3	152	Truro	-4.7	0.31	-1.99	-4.31	75°13.94'N, 97°00.24'W
2001	154	Truro	-1.5	0.19	-1.44	-3.8	4.7	154	Truro	-1.59	0.31	-1.99	-4.03	75°13.94'N, 97°00.24'W
2001	156	Truro	-0.8	0.17	-1.38	-3.5	4.4	156	Truro	-4.21	0.31	-1.99	-3.89	75°13.94'N, 97°00.24'W
2001	158	Truro	1.4	0.15	-1.41	-3.1	4.5	158	Truro	-2.29	0.31	-2.00	-3.62	75°13.94'N, 97°00.24'W
2001	160	Truro	-1.5	0.22	-1.45	-2.9	4.7	160	Truro	0.24	0.26	-2.00	-3.39	75°13.94'N, 97°00.24'W
2001	162	Truro	-1.0	0.15	-1.35	-2.7	4.8	162	Truro	-1.6	0.18	-2.00	-3.23	75°13.94'N, 97°00.24'W
2001	173	Truro	2.3	0.05	-1.34	-1.1		173	Truro	-3.66	0.00	-1.67	-1.39	75°13.94'N, 97°00.24'W
2002	122	122_Bar		0.07		-8.99	5.50	122	Barrow	-7.63	0.12	-2.18	-9.92	74°51'10.5" N, 97°07'41.4"'

									(B1)					W
2002	143	143_Truro		0.15	-1.55	-5.58	4.98							
2002	149	149_Truro	-3.3	0.14	-1.43	-3.31	5.70	149	Truro	-2.72	0.11	-2.17	-3.75	74°54.69' N, 97° 13.33' W
2002	156	156_Truro		0.13	-1.46	-2.70	5.46	156	Truro	-2.86	0.04	-2.17	-2.48	74°54.69' N, 97° 13.33' W
2002	157	157_Bar	-1	0.07	-1.87	-3.21	5.00	157	Barrow (B3)	-2.53	0.13	-2.27	-3.86	74° 50.72' N, 97°07.50' W
2002	157	157_Leo	0.5	0.14	-1.51	-1.99	6.28	157	Leopold (L2)	-2.46	0.13	-2.26	-3.84	74° 18.26' N, 91° 05.46' W
2002	157	157_Grif	1.7	0.09	-1.37	-1.12	5.94	157	Griffith (G2)	-2.26	0.13	-2.27	-3.75	74° 21.19' N, 94°56.10' W
2002	165	165_AB(l)	3.4	0.02	-2.07		4.06	165	AB(1)	2	0.00	-2.26	-2.39	74°43.97' N, 95°15.00' W
2002	166	166_Bar	4	0.04	-2.15	-1.70	3.87							
2002	166	166_Leo		0.05	-1.69	-1.23	4.56							
2002	167	167_Grif		0.03	-1.33	-0.95	4.49							
2002	168	168_AB(l)	4.3	0.00	-2.01			168	AB(1)	3.67	0.00	-2.14	-1.98	74°43.97' N, 95°15.00' W
2002	168	168_AB(M)		0.01	-2.24		3.87							
2002	171	171_AB(l)		0.00				171	AB(1)	2.98	0.00	-2.00	-1.66	74°43.97' N, 95°15.00' W
2002	175	175_Bar	4.3	0.02	-1.90	-1.47	4.41							
2002	175	175_Grif	4.3	0.03	-1.30	-0.88	3.74							
2002	175	175_Truro		0.03	-1.43	-1.11	4.10	175	Truro	-0.32	0.00	-1.37	-0.9	74°54.69' N, 97° 13.33' W
2002	175	175_AB(l)		0.02	-1.86		3.25	175	AB(1)	2.19	0.00	-1.76	-1.34	74°43.97' N, 95°15.00' W
2002	180	180_Truro		0.05	-1.24	-1.11	4.06	180	Truro	2.99	0.00	-0.98	-0.71	74°54.69' N, 97° 13.33' W
2002	183	183_Truro		0.04	-1.08	-0.60	3.60	183	Truro	2.44	0.00	-0.70	-0.62	74°54.69' N, 97° 13.33' W
2002	186	186_Truro		0.03	-1.11	-1.18	3.20	186	Truro	-1.65	0.00	-0.40	-0.55	74°54.69' N, 97° 13.33' W
2002	207	207_AB1(l)		0.00	-1.19		0.13	207	AB(2)	2.09	0.00	0.00	1.25	74°43.23' N, 95°04.46' W
2002	207	207_AB2(l)		0.00	-0.85		0.03							
2002	223	223_CAB		0.00	-1.27		0.46	223	AB(3)	3.29	0.00	0.00	3.85	74°46.15' N, 95°17.29' W

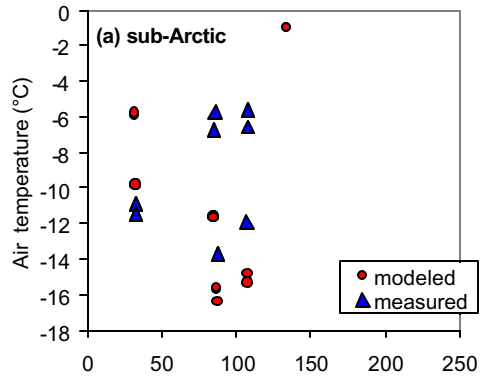
(a) sub-Arctic
Air temperature (°C)
0
-2
-4
-6
-8
-10
-12
-14
-16
-18
0
50
100
150
200
250
modeled
measured

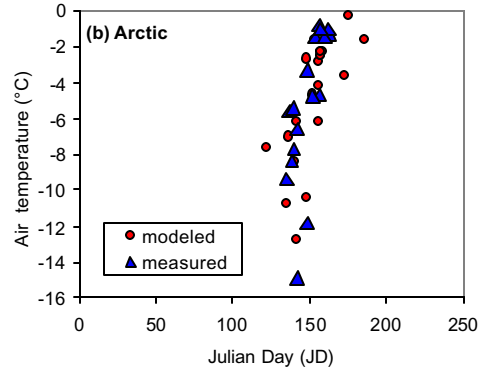
(b) Arctic
Air temperature (°C)
0
-2
-4
-6
-8
-10
-12
-14
-16
0
50
100
150
200
250
Julian Day (JD)
modeled
measured

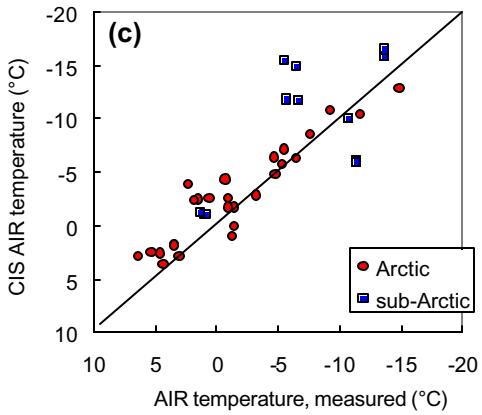
(c)
CIS AIR temperature (°C)
-20
-15
-10
-5
0
5
10
10
5
0
-5
-10
-15
-20
AIR temperature, measured (°C)
Arctic
sub-Arctic

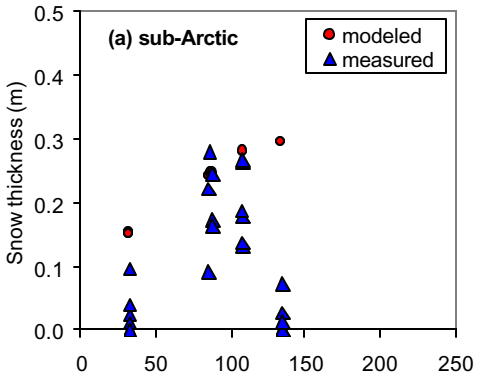
(a) sub-Arctic
Snow thickness (m)
0.5
0.4
0.3
0.2
0.1
0.0
0
50
100
150
200
250
modeled
measured

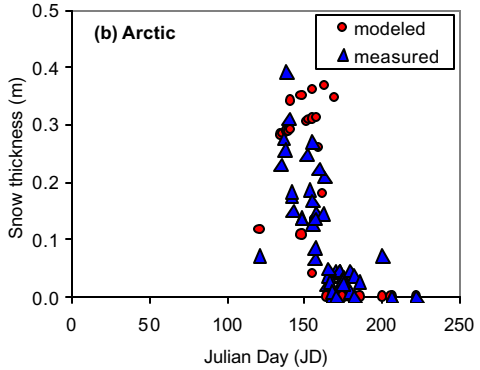
(b) Arctic
Snow thickness (m)
0.5
0.4
0.3
0.2
0.1
0.0
0
50
100
150
200
250
Julian Day (JD)
modeled
measured

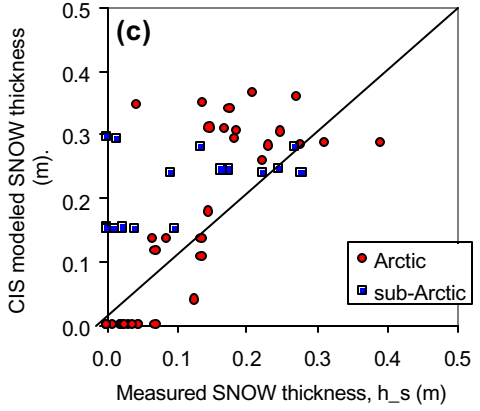
(c)
CIS modeled SNOW thickness (m).
0.5
0.4
0.3
0.2
0.1
0.0
0.0
0.1
0.2
0.3
0.4
0.5
Measured SNOW thickness, h_s (m)
Arctic
sub-Arctic

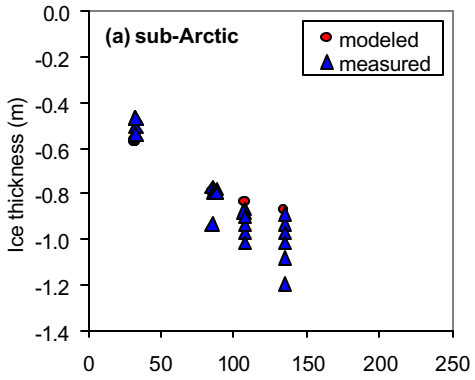
(a) sub-Arctic
modeled
measured
Ice thickness (m)
0.0
-0.2
-0.4
-0.6
-0.8
-1.0
-1.2
-1.4
0
50
100
150
200
250

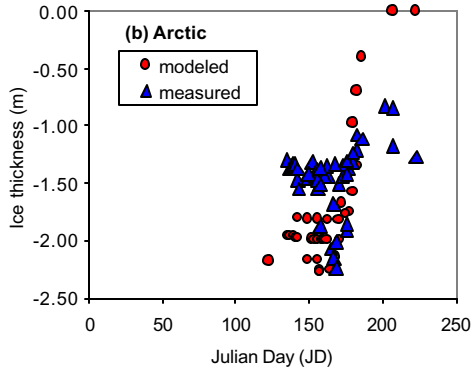
(b) Arctic
modeled
measured
Ice thickness (m)
0.00
-0.50
-1.00
-1.50
-2.00
-2.50
0
50
100
150
200
250
Julian Day (JD)

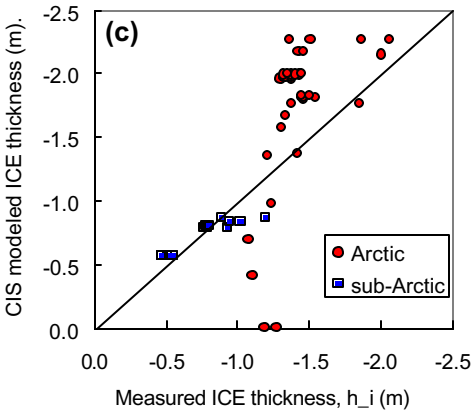
(c)
Arctic
sub-Arctic
CIS modeled ICE thickness (m).
-2.5
-2.0
-1.5
-1.0
-0.5
0.0
0.0
-0.5
-1.0
-1.5
-2.0
-2.5
Measured ICE thickness, h_i (m)

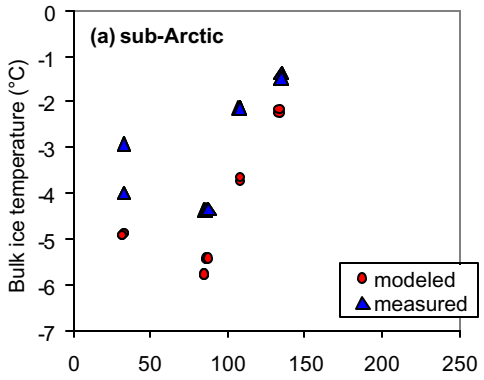
(a) sub-Arctic
modeled
measured
Bulk ice temperature (°C)
0
-1
-2
-3
-4
-5
-6
-7
0
50
100
150
200
250

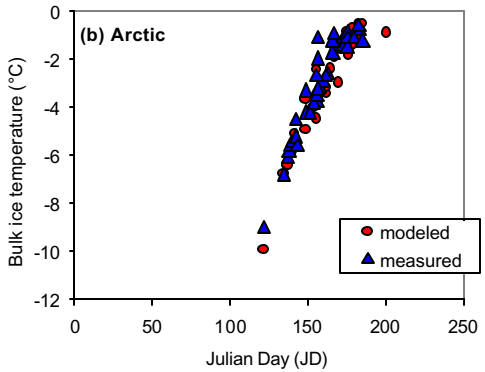
(b) Arctic
modeled
measured
Bulk ice temperature (°C)
0
-2
-4
-6
-8
-10
-12
0
50
100
150
200
250
Julian Day (JD)

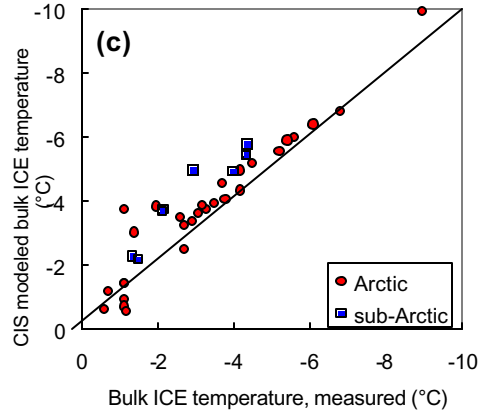
(c)
Arctic
sub-Arctic
CIS modeled bulk ICE temperature (°C)
-10
-8
-6
-4
-2
0
0
-2
-4
-6
-8
-10
Bulk ICE temperature, measured (°C)

Appendix C: Field Measurements vs. Forecasted Data from CIS Model

Table C-1 Comparison of Flexural Strength Calculated using Approach A and Approach D

			MODELED		MEASURED	
Year	JD	Site	FS (MPa)	sqrt brine fraction	FS (MPa)	sqrt brine fraction
sub-Arctic						
2004	33	S2	0.40	0.25	0.40	0.25
2004	33	S6	0.40	0.25	0.40	0.25
2004	33	S10	0.40	0.25	0.40	0.25
2004	85	S2	0.43	0.24	0.38	0.26
2004	85	S6	0.43	0.24	0.44	0.23
2004	86	S10	0.42	0.25	0.41	0.25
2004	108	S2	0.30	0.30	0.27	0.32
2004	108	S6	0.30	0.30	0.23	0.35
2004	108	S10	0.30	0.30	0.26	0.33
2004	134	S2	0.20	0.37	0.16	0.41
2004	134	S6	0.20	0.37	0.13	0.45
2004	134	S10	0.20	0.37	0.15	0.42
2004	32	A2	0.40	0.25	0.28	0.31
2004	32	A6	0.40	0.25	0.27	0.32
2004	32	A10	0.40	0.25	0.20	0.37
2004	87	A2	0.42	0.25	0.45	0.23
2004	87	A6	0.42	0.25	0.40	0.25
2004	88	A10	0.42	0.24	0.47	0.22
2004	108	A2	0.30	0.30	0.23	0.35
2004	108	A6	0.30	0.30	0.25	0.33
2004	108	A10	0.30	0.30	0.28	0.31
2004	134	A2	0.20	0.37	0.13	0.44
2004	134	A6	0.20	0.37	0.16	0.41
2004	134	A10	0.20	0.37	0.19	0.38
Arctic						
2000	142	Truro	0.53	0.20	0.40	0.06
2000	149	Truro	0.52	0.21	0.34	0.08
2000	156	Truro	0.49	0.22	0.35	0.07
2000	163	Truro	0.43	0.24	0.25	0.11
2000	170	Truro	0.38	0.26	0.17	0.16
2000	173	Truro			0.17	0.16
2000	177	Truro	0.31	0.29		
2000	180	Truro	0.24	0.34	0.16	0.16
2000	183	Truro	0.19	0.38		
2000	201	Truro		0.60		
2001	135	Truro	0.58	0.19	0.57	0.04
2001	137	Truro	0.56	0.19	0.51	0.04
2001	138	Truro			0.51	0.05
2001	139	Truro	0.54	0.20	0.49	0.05
2001	140	Truro	0.54	0.20	0.54	0.04
2001	142	Truro	0.53	0.21	0.47	0.05
2001	152	Truro	0.46	0.23	0.46	0.05
2001	154	Truro	0.44	0.23	0.40	0.06
2001	156	Truro	0.43	0.24	0.40	0.06
2001	158	Truro	0.41	0.25	0.36	0.07

2001	160	Truro	0.39	0.25	0.33	0.08
2001	162	Truro	0.38	0.26	0.30	0.09
2001	173	Truro	0.30	0.30		
2002	122	Bar	0.66	0.17	0.60	0.03
2002	143	Truro			0.49	0.05
2002	149	Truro	0.51	0.21	0.31	0.09
2002	156	Truro	0.43	0.24	0.27	0.10
2002	157	Bar	0.44	0.24	0.34	0.08
2002	157	Leo	0.41	0.25	0.17	0.16
2002	157	Grif	0.43	0.24	0.09	0.26
2002	165	AB(l)	0.37	0.27		
2002	166	Bar			0.24	0.11
2002	166	Leo			0.14	0.18
2002	167	Grif			0.10	0.23
2002	168	AB(l)	0.34	0.28		
2002	168	AB(M)				
2002	171	AB(l)	0.26	0.32		
2002	175	Bar			0.18	0.15
2002	175	Grif			0.12	0.21
2002	175	Truro	0.24	0.34	0.14	0.18
2002	175	AB(l)	0.20	0.37		
2002	180	Truro	0.19	0.38	0.14	0.18
2002	183	Truro	0.16	0.41	0.07	0.30
2002	186	Truro	0.13	0.44	0.20	0.14
2002	207	AB1(l)	0.77			
2002	207	AB2(l)				
2002	223	CAB		0.00		